A systematic approach for the Jacobian analysis of parallel manipulators with two end-effectors

Hoevenaars, A. G L; Gosselin, C.; Lambert, P.; Herder, J. L.

DOI
10.1016/j.mechmachtheory.2016.10.022

Publication date
2017

Document Version
Final published version

Published in
Mechanism and Machine Theory

Mechanism and Machine Theory 109 (2017) 171–194

Contents lists available at ScienceDirect

Mechanism and Machine Theory

journal homepage: www.elsevier.com/locate/mechmachtheory

A Systematic Approach for the Jacobian Analysis of Parallel Manipulators with Two End-Effectors

A.G.L. Hoevenaars[a,*], C. Gosselin[b], P. Lambert[a], J.L. Herder[a]

[a] Faculty of Mechanical, Maritime and Materials Engineering, Delft University of Technology, 2628 CD Delft, The Netherlands
[b] Department of Mechanical Engineering, Laval University, Québec G1V 0A6, Canada

ARTICLE INFO

Keywords:
Parallel manipulators
Gripping
Two end-effectors
Configurable platform
Jacobian analysis
Screw theory

ABSTRACT

Parallel manipulators with two end-effectors (PM2Es) enable the design of gripping robots with high dynamic performance. The gripping action is enabled by internal, relative degrees of freedom (DoFs) between the two end-effectors. Many standard methods for the analysis and control of parallel manipulators rely on a Jacobian, where a complete Jacobian analysis includes constraint relations. These constraint relations have not been consistently included in previous analyses of PM2Es, while they are specifically relevant for PM2Es because constraints play an important role in the static force analysis of a PM2E. This is because wrenches applied by the actuators can be transferred to the end-effectors through internal constraints, an effect which is not captured by kinematic relations alone. This paper presents a systematic approach to perform the Jacobian analysis of PM2Es, which is based on screw theory, and that takes all constraint relations into account. The approach is applied to a PM2E with three legs and one internal closed-loop chain. An example mechanism was built to experimentally validate the resulting Jacobian analysis using a static force analysis.

1. Introduction

Gripping is an important aspect of many modern robotic systems, such as pick-and-place robots [1,2], microassembly robots [3,4], and haptic devices [5,6]. An important category of grippers are those which mechanically engage an object in a multi-point contact [7,8].

For many applications a driving requirement is dynamic performance, which asks for robotic systems with a high stiffness-over-inertia ratio. Despite their advantageous stiffness-over-inertia ratio, only few mechanically gripping robots are based on parallel manipulators (PMs). A PM can have all actuators located at the base, which significantly reduces the effective inertia. However, the standard solution for adding a gripping capability to a PM is to connect an additional, dedicated gripper in series to the end-effector as, for example, in Ref. [3]. Because of its placement at the end-effector, the inertia of a gripper can significantly degrade the dynamic performance of the resulting manipulator.

Parallel manipulators with two end-effectors (PM2Es) are a relatively novel class of PMs and form a promising alternative solution for gripping robots. PM2Es are an interpretation of parallel manipulators with a configurable platform [6,10–14], where a closed-loop chain replaces the rigid platform of a traditional PM. This architecture enables the design of gripping robots with all motors located at the base, which is beneficial for the overall dynamic performance. The first example of such gripping robot was

* Corresponding author.
E-mail addresses: a.g.l.hoevenaars@tudelft.nl (A.G.L. Hoevenaars), clement.gosselin@gmc.ulaval.ca (C. Gosselin), p.lambert@tudelft.nl (P. Lambert), j.l.herder@tudelft.nl (J.L. Herder).

http://dx.doi.org/10.1016/j.mechmachtheory.2016.10.022
Received 2 May 2016; Received in revised form 25 October 2016; Accepted 27 October 2016
Available online 04 December 2016
0094-114X/

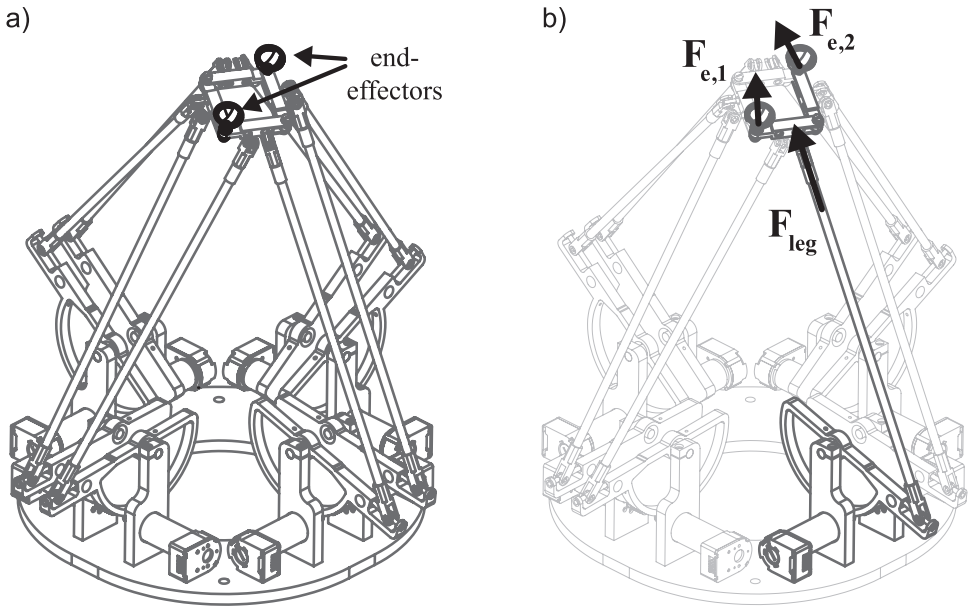

Fig. 1. a) A parallel manipulator with two end-effectors (PM2E) interacts with the environment via two specific bodies, where b) wrenches applied by the legs can be transferred to the end-effectors through internal constraints.

introduced by Yi et al. [10], where the whole closed-loop chain acts as the gripper. This paper focuses on PMCPs where two specific bodies of the closed-loop chain interact with the environment, which is illustrated in Fig. 1 for the overactuated 7-DoF haptic master device introduced by Lambert and Herder [6]. Therefore, the term PM2E is preferred.

For the analysis and control of PMs a Jacobian is used [15–18] and therefore various researchers have focused on the Jacobian analysis of PM2Es. Yi et al. [10] differentiated the inverse kinematic relations to obtain an expression for the Jacobian. Mohamed and Gosselin [9] performed a Jacobian analysis based on a set of loop-closure equations that must be solved simultaneously. Lambert et al. [13] applied a stepwise approach in which they first obtained an expression for the motion of the connection point of each *leg*, which is a serial chain that connects the internal closed-loop chain to the base as illustrated in Fig. 2a. They then developed a Jacobian based on the relations between allowed end-effector motions, motions of the leg connection points and motions of the actuators. Nabat et al. [12] considered the end-effector velocity state of their manipulator as the combination of a platform twist and an additional velocity term to represent the internal platform motion.

More recently, Hoevenaars et al. [19] made a first attempt to generalize the Jacobian analysis of PM2Es based on screw theory

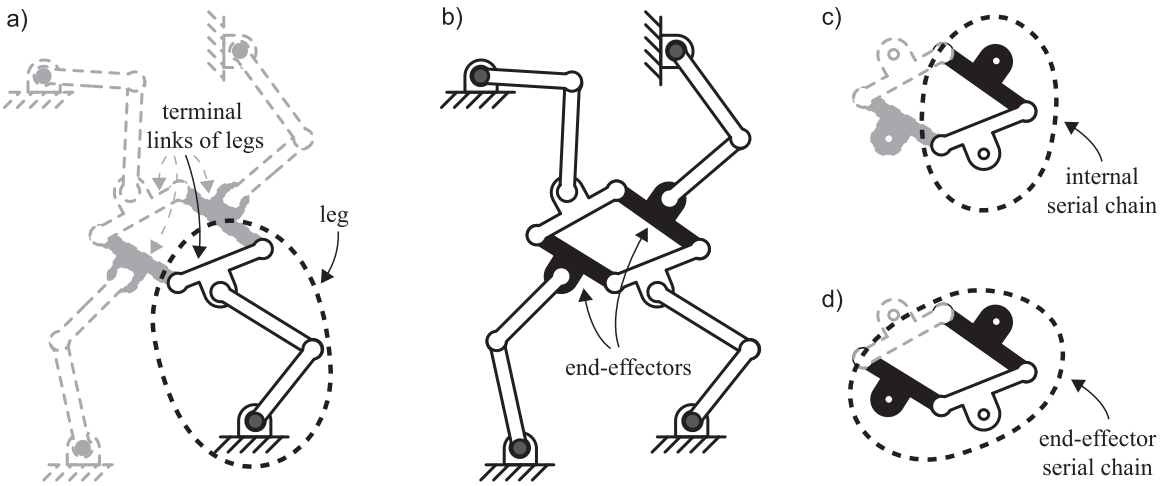

Fig. 2. A planar manipulator as described in Ref. [9], for which are indicated a) the terminal links of the different legs, b) the fact that two terminal links need to be designated as end-effectors, c) one of the four internal serial chain, and d) one of two end-effector serial chain.

and using a mapping of a set of twists. The resulting Jacobian analysis expresses the velocity state of a spatial PM2E as a combination of two twists with respect to the ground, one for each end-effector. As opposed to other analyses, the analysis in Ref. [19] does include constraint relations, but not those within the internal closed-loop chain.

However, internal constraint relations can be particularly relevant for PM2Es, because wrenches applied by the legs can be transferred to the end-effectors through internal constraints, as illustrated in Fig. 1b. As such, an incomplete consideration of constraint relations can make the obtained Jacobian analysis invalid for use in a static force analysis. Because gripping is mainly a force task, a static force analysis is of particular interest in gripping robots. Therefore, the absence of a Jacobian analysis that is also valid for use in a static force analysis represents a significant gap in the existing knowledge of PM2Es.

The aim of this paper is to develop a systematic approach for the Jacobian analysis of PM2Es. Special attention will be given to the analysis of constraints so that the resulting Jacobian can be used in a static force analysis. Constraint relations in a Jacobian can also be relevant in a stiffness analysis [20,21].

The structure of this paper is as follows. First, definitions and assumptions are introduced, which will be used throughout this paper. Then, a novel structure for the Jacobian analysis of PM2Es with an internal closed-loop chain is developed, which maps the set of all terminal link twists on the joint velocities of all serial chains. Next, for the example of a three-legged PM2E with an internal closed-loop chain the matrix which maps the two end-effector twists on the set of all terminal link twists is developed. An example Jacobian analysis is performed for a three-legged PM2E by combining the novel structure with the mapping of end-effector twists. An experimental static force analysis is performed to validate this Jacobian analysis.

2. Definitions and assumptions

This paper focuses on PM2Es with a single internal closed-loop chain. This internal closed-loop chain can impose constraints on the relative motion between the two end-effectors, while the legs may impose additional constraints. All twists introduced in this paper are expressed in a Cartesian reference frame attached to the body in question. Each twist is expressed as $\$_t = [\boldsymbol{\omega}^\top \quad \boldsymbol{v}^\top]^\top$, where $\boldsymbol{\omega}$ is the angular velocity vector and $\boldsymbol{v}$ is the velocity vector of the body, expressed in the Cartesian reference frame. The linear operator that maps $\$_t$ on the scalar representing power is the transpose of the wrench defined as $\$_w = [\boldsymbol{m}^\top \quad \boldsymbol{f}^\top]^\top$, where $\boldsymbol{m}$ and $\boldsymbol{f}$ are the moment and force applied at the point that coincides with the origin of the Cartesian reference frame of the body in question.

A number of additional definitions and related assumptions are used throughout this paper, namely:

- **Terminal link.** The rigid body of a leg which is also part of the internal closed-loop chain is termed the leg's terminal link, see Fig. 2a. The terminal link of the leg i is labeled n_i.
- **Internal serial chain.** Each serial chain connecting two adjacent terminal links will be referred to as an internal serial chain. See Fig. 2c for an example.
- **End-effector serial chain.** The closed-loop chain of a PM2E can also be considered as two serial chains connecting the two end-effectors in parallel. Each of these serial chains will be referred to as an end-effector serial chain and contains one or more internal serial chains. It is assumed that there are no redundant joints in each end-effector serial chain. This concept will be important for later derivations. See Fig. 2d for an example.
- **Connectivity.** Similar to Joshi and Tsai [22], it is assumed that the number of degrees of freedom of a serial chain, referred to as its connectivity C, corresponds to the number of kinematic joints in that serial chain. It is assumed that this also holds for each end-effector serial chain, so that also within an end-effector serial chain there are no redundant joints.
- **Virtual joint.** If a serial chain has $C < 6$, then $6 - C$ basis twists are constrained. Each basis twist represents the motion of a 1-DoF joint, and since the joints associated to constrained twists are not part of the kinematic chain, they are termed virtual joints. See Ref. [21] for more details.

3. Structure for novel jacobian analysis of PM2Es

In this section a novel structure for the Jacobian analysis of PM2Es with a single internal closed-loop chain is presented. The main idea is to organize the partial inverse Jacobian matrices of individual serial chains based on the structure in the graph representation. The resulting Jacobian analysis is a function of the twists of the various terminal links.

At the basis of existing Jacobian analysis methods for traditional PMs lies the structured combination of inverse Jacobian matrices of individual legs,

$$\begin{bmatrix} \dot{\boldsymbol{q}}_1 \\ \dot{\boldsymbol{q}}_2 \\ \vdots \\ \dot{\boldsymbol{q}}_N \end{bmatrix} = \begin{bmatrix} \mathbf{J}_1^{-1} \\ \mathbf{J}_2^{-1} \\ \vdots \\ \mathbf{J}_N^{-1} \end{bmatrix} \$_{t,e} \tag{1}$$

where N is the number of legs and $\$_{t,e}$ is the twist of the end-effector. Also, if the full inverse Jacobian analysis is considered as in Ref. [23], for each leg i the matrix $\mathbf{J}_i^{-1}$ is a 6×6 inverse Jacobian matrix and each vector $\dot{\boldsymbol{q}}_i$ is a six-dimensional vector that contains both kinematic joint velocities and virtual joint velocities of a leg. Kinematic joint velocities include actuated joints and passive joints. Any component of $\$_{t,e}$ that is mapped onto virtual joint velocities therefore implies that there are deformations in the manipulator.

The inclusion of virtual joints, as well as passive joints, is for example important for singularity analysis [16] and is also used in

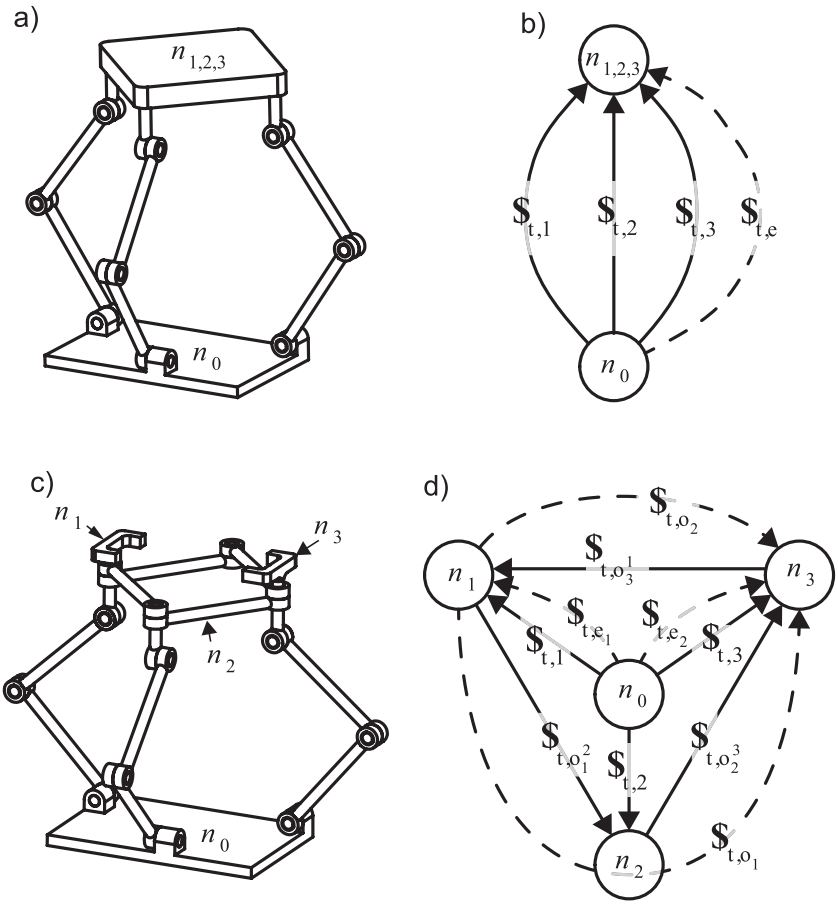

Fig. 3. a) An example of a traditional PM with three legs and b) its graph theory representation, as well as c) an example of a PM2E with three legs as introduced in Ref. [24] and d) its graph theory representation.

Jacobian-based stiffness analyses [20,21]. Nonetheless, if the mapping onto virtual joints and/or passive joints is not of interest, the rows responsible for this mapping can be removed from the full inverse Jacobian matrix.

In this paper the full inverse Jacobian analysis as introduced in Ref. [23] is extended to PM2Es. Therefore, it is helpful to look at the difference between the graph representations of traditional PMs and PM2Es. Fig. 3 shows a three-legged PM and an example of a three-legged PM2E, both with their respective graphs. For each twist, the arrow points from the reference body to the body moving relative to it. Overlaid with dotted lines are the known end-effector twists, $\$_{t,e}$ in Fig. 3 b and $\$_{t,e1}$ and in Fig. 3 d$\$_{t,e2}$, as well as the twists related to the two end-effector serial chains, $\$_{t,o1}$ and $\$_{t,o2}$.

Firstly, in order to compare the associated Jacobian matrices, the twist of the terminal link of each leg i of a traditional PM is expressed as $\$_{t,i}$ instead of $\$_{t,e}$, so that Eq. (1) can be rewritten as

$$\begin{bmatrix} \dot{\boldsymbol{q}}_1 \\ \dot{\boldsymbol{q}}_2 \\ \vdots \\ \dot{\boldsymbol{q}}_N \end{bmatrix} = \begin{bmatrix} \mathbf{J}_1^{-1} & \mathbf{0}_{6\times6} & \dots & \mathbf{0}_{6\times6} \\ \mathbf{0}_{6\times6} & \mathbf{J}_2^{-1} & \dots & \mathbf{0}_{6\times6} \\ \vdots & \vdots & \ddots & \vdots \\ \mathbf{0}_{6\times6} & \mathbf{0}_{6\times6} & \dots & \mathbf{J}_N^{-1} \end{bmatrix} \begin{bmatrix} \$_{t,1} \\ \$_{t,2} \\ \vdots \\ \$_{t,N} \end{bmatrix} \tag{2}$$

where for a traditional PM it thus holds that

$$\$_{t,i} = \$_{t,e} \tag{3}$$

so that Eq. (2) can be simplified to Eq. (1). On the other hand, for a PM2E Eq. (3) does not hold since the twists of the terminal links are not all the same.

A second difference with traditional PMs is that a PM2E with N legs and a single closed-loop chain in addition has N internal serial chains. Each internal serial chain connects two terminal links, so that the twist of each internal serial chain can be expressed as

$$\$_{t,o_i^{i+1}} = \begin{cases} \$_{t,i+1} - \$_{t,i} & \text{for} i = 1, 2, \ldots, (N-1) \\ \$_{t,1} - \$_{t,N} & \text{for} i = N \end{cases} \tag{4}$$

where $\$_{t,o_i^{i+1}}$ is the twist of the internal serial chain connecting the ith terminal link with the $(i+1)$ th terminal link. Eq. (4) states that the Nth terminal link is connected to the first terminal link.

The full Jacobian analysis of a PM2E can therefore be obtained by extending Eq. (2) with the relations described by Eq. (4),

$$\begin{bmatrix} \dot{\boldsymbol{q}}_1 \\ \dot{\boldsymbol{q}}_2 \\ \vdots \\ \dot{\boldsymbol{q}}_N \\ \dot{\boldsymbol{q}}_{o_1^2} \\ \dot{\boldsymbol{q}}_{o_2^3} \\ \vdots \\ \dot{\boldsymbol{q}}_{o_N^1} \end{bmatrix} = \mathbf{J}_n^{-1} \begin{bmatrix} \$_{t,1} \\ \$_{t,2} \\ \vdots \\ \$_{t,N} \end{bmatrix} \tag{5}$$

where $\dot{\boldsymbol{q}}_{o_i^{i+1}}$ (or $\dot{\boldsymbol{q}}_{o_N^1}$) is the six-dimensional joint velocity vector of the i th internal serial chain, and

$$\mathbf{J}_n^{-1} = \begin{bmatrix} \mathbf{J}_1^{-1} & \mathbf{0}_{6\times6} & \cdots & \mathbf{0}_{6\times6} \\ \mathbf{0}_{6\times6} & \mathbf{J}_2^{-1} & \cdots & \mathbf{0}_{6\times6} \\ \vdots & \vdots & \ddots & \vdots \\ \mathbf{0}_{6\times6} & \mathbf{0}_{6\times6} & \cdots & \mathbf{J}_N^{-1} \\ -\mathbf{J}_{o_1^2}^{-1} & \mathbf{J}_{o_1^2}^{-1} & \cdots & \mathbf{0}_{6\times6} \\ \mathbf{0}_{6\times6} & -\mathbf{J}_{o_2^3}^{-1} & \cdots & \mathbf{0}_{6\times6} \\ \vdots & \vdots & \ddots & \vdots \\ \mathbf{J}_{o_N^1}^{-1} & \mathbf{0}_{6\times6} & \cdots & -\mathbf{J}_{o_N^1}^{-1} \end{bmatrix} \tag{6}$$

where the matrices $\mathbf{J}_{o_i^{i+1}}^{-1}$ (or $\mathbf{J}_{o_N^1}^{-1}$) are the result of including the mappings from the relative twists of Eq. (4) onto the joint velocities of the internal serial chains. As in Eq. (1), each of the inverse Jacobian matrices in Eq. (6) is a 6×6 matrix and can be obtained using the reciprocity rules of twists and wrenches as described in Ref. [23]. In short, the complex kinematic structure of a PM2E has been reduced to an organized combination of serial chains with known twists, which is also at the basis of the inverse Jacobian analysis of traditional parallel manipulators.

As opposed to a traditional PM, the twist of each terminal link of a PM2E can be different. And because typically only the twists of the two terminal links that are the end-effectors are directly available as inputs, not all twists in Eq. (5) are directly defined. This is the topic of the next section.

4. Mapping of twists for three-legged PM2E

In this section the matrix is developed that maps the two end-effector twists onto the complete set of terminal link twists for the example of a PM2E with three legs, whose graph representation was already introduced in Fig. 3d. Thus, a matrix $\mathbf{M}_t$ is developed such that

$$\begin{bmatrix} \$_{t,1} \\ \$_{t,2} \\ \$_{t,3} \end{bmatrix} = \mathbf{M}_t \begin{bmatrix} \$_{t,e_1} \\ \$_{t,e_2} \end{bmatrix} \tag{7}$$

In the example considered in this paper the terminal links of the first and third leg, n_1 and n_3, are the end-effectors, so that

$$\$_{t,1} = \$_{t,e_1} \quad \$_{t,3} = \$_{t,e_2} \tag{8}$$

and the difficulty in developing $\mathbf{M}_t$ for this example lies in the mapping of the two end-effector twists onto $\$_{t,2}$.

To enable a mapping of the two end-effector twists onto $\$_{t,2}$, either $\$_{t,o_1^2}$ or $\$_{t,o_2^3}$ needs to be expressed, because from Fig. 3d it can be established that

$$\$_{t,2} = \$_{t,1} + \$_{t,o_1^2} \tag{9}$$

and also

$$\$_{t,2} = \$_{t,3} - \$_{t,o_2^3} \tag{10}$$

To express $\$_{t,o_1^2}$ or $\$_{t,o_2^3}$, this paper first develops a set of basis twists to express $\$_{t,o_1}$, which is here defined as the twist of the end-effector serial chain that connects n_1 and n_3 via n_2, see Fig. 3d. In the remainder of this research, this end-effector serial chain will be referred to as the first end-effector serial chain (and as a logical consequence, the other end-effector serial chain will be referred to as

the *second end-effector serial chain*). It was assumed that the number of kinematic joints in each end-effector serial chain is equal to its connectivity, where the connectivity of the first end-effector serial chain is labeled C_{o_1}. Then it holds that

$$C_{o_1} = C_{o_1^2} + C_{o_2^3} \tag{11}$$

where $C_{o_1^2}$ is the connectivity of the internal serial chain connecting n_1 and n_2, and $C_{o_2^3}$ is the connectivity of the internal serial chain connecting n_2 and n_3. The twist $\$_{t,o_1}$ can then be expressed as

$$\$_{t,o_1} = \sum_{j=1}^{C_{o_1^2}} \dot{q}_{a,o_{1,j}} \hat{\$}_{ta_{o_{1,j}}} + \sum_{j=1}^{C_{o_2^3}} \dot{q}_{a,o_{1,j^*}} \hat{\$}_{ta_{o_{1,j^*}}} + \sum_{j=1}^{6-C_{o_1}} \dot{q}_{c,o_{1,j}} \hat{\$}_{tc_{o_{1,j}}} \tag{12}$$

where

$$j^* = j + C_{o_1^2} \tag{13}$$

is introduced to shorten the notation, and $\hat{\$}_{ta_{o_{1,j}}}$ is the unit twist of permission associated to the j th joint of the first end-effector serial chain, with $\dot{q}_{a,o_{1,j}}$ its magnitude. The unit twist of restriction $\hat{\$}_{tc_{o_{1,j}}}$ represents the motion of the jth virtual joint of the first end-effector serial chain, with magnitude $\dot{q}_{c,o_{1,j}}$. These six unit twists together span six-dimensional Cartesian space.

Next, the set of unit twists introduced in Eq. (12) is also used to express $\$_{t,o_1^2}$ and $\$_{t,o_2^3}$. However, each unit twists of permission in Eq. (12) is constrained in one of the internal serial chains. Therefore, this paper makes a distinction between three types of unit twists, expressed using their magnitudes:

- **Permitted twist magnitudes.** The unit twists associated to joints that represent a kinematic DoF of the considered internal serial chain are given a magnitude $\dot{q}_{a,o_i^{i+1},j}$.
- **Simple constrained internal twist magnitudes.** The unit twists associated to joints that represent a constraint in the considered internal serial chain, but which represent a kinematic DoF in the first end-effector serial chain, are simple constrained internal twists. These twists are given a magnitude $\dot{q}_{c_s,o_i^{i+1},j}$.
- **Multiple constrained internal twist magnitudes.** The unit twists associated to joints that represent a constrained DoF in the first end-effector serial chain necessarily also represent a constrained DoF in both internal serial chains of which it is constructed. These twists are therefore multiple constrained and in the considered internal serial chain are attributed a magnitude $\dot{q}_{c_m,o_i^{i+1},j}$.

With the distinction as above, each internal joint velocity vector is then constructed as

$$\dot{\boldsymbol{q}}_{o_i^{i+1}} = \begin{bmatrix} \dot{\boldsymbol{q}}_{a,o_i^{i+1}} \\ \dot{\boldsymbol{q}}_{c_s,o_i^{i+1}} \\ \dot{\boldsymbol{q}}_{c_m,o_i^{i+1}} \end{bmatrix} \tag{14}$$

Now, $\$_{t,o_1^2}$ and $\$_{t,o_2^3}$ can be expressed respectively as

$$\$_{t,o_1^2} = \sum_{j=1}^{C_{o_1^2}} \dot{q}_{a,o_1^2,j} \hat{\$}_{ta_{o_{1,j}}} + \sum_{j=1}^{C_{o_2^3}} \dot{q}_{c_s,o_1^2,j} \hat{\$}_{ta_{o_{1,j^*}}} + \sum_{j=1}^{6-C_{o_1}} \dot{q}_{c_m,o_1^2,j} \hat{\$}_{tc_{o_{1,j}}} \tag{15}$$

and

$$\$_{t,o_2^3} = \sum_{j=1}^{C_{o_2^3}} \dot{q}_{a,o_2^3,j} \hat{\$}_{ta_{o_{1,j^*}}} + \sum_{j=1}^{C_{o_1^2}} \dot{q}_{c_s,o_2^3,j} \hat{\$}_{ta_{o_{1,j}}} + \sum_{j=1}^{6-C_{o_1}} \dot{q}_{c_m,o_1^2,j} \hat{\$}_{tc_{o_{1,j}}} \tag{16}$$

where j^* was introduced in Eq. (13). The remaining challenge is to obtain expressions for all twist magnitudes in either Eq. (15) or Eq. (16).

To express the twist magnitudes in Eqs. (15) and (16) velocity relations are derived from the knowledge that the sum of all twists in a closed loop is zero. Therefore, as can be observed from Fig. 3d, for a PM2E with three legs it holds among others that

$$\$_{t,o_1^2} + \$_{t,o_2^3} + \$_{t,o_3^1} = 0 \tag{17}$$

Additionally, using another loop, $\$_{t,o_3^1}$ can be expressed as

$$\$_{t,o_3^1} = \$_{t,1} - \$_{t,3} \tag{18}$$

and because Eq. (8), it is possible to combine Eqs. (17) and (18) into

$$\$_{t,e_2} - \$_{t,e_1} = \$_{t,o_1^2} + \$_{t,o_2^3} \tag{19}$$

Furthermore, because the first end-effector serial chain was defined as the combination of the internal serial chain connecting n_1 and n_2, and the internal serial chain connecting n_2 and n_3, it also holds that

$$\$_{t,e_2} - \$_{t,e_1} = \$_{t,o_1} \tag{20}$$

4.1. Expression for actuated and simple constrained joint velocities in the first end-effector serial chain

In this subsection expressions are derived for $\dot{\boldsymbol{q}}_{a,o_1^2}$, $\dot{\boldsymbol{q}}_{c_s,o_1^2}$, $\dot{\boldsymbol{q}}_{a,o_2^3}$, and $\dot{\boldsymbol{q}}_{c_s,o_2^3}$, as introduced in Eq. (14), using the method and notation as introduced in Ref. [23]. These expressions are necessary for later steps in the proposed analysis and are based on the definition of the first end-effector serial chain as the series connection of two internal serial. Thus, each of the kinematic joints in the first end-effector serial chain is part of either the internal serial chain connecting n_1 and n_2, or the internal serial chain connecting n_2 and n_3, and therefore it holds that

$$\dot{q}_{a,o_{1,j}} = \dot{q}_{a,o_1^2,j} \quad \text{for} j = 1, 2, \ldots C_{o_1^2} \tag{21}$$

$$\dot{q}_{a,o_{1,j^*}} = \dot{q}_{a,o_2^3,j} \quad \text{for} j = 1, 2, \ldots C_{o_2^3} \tag{22}$$

where j^* was expressed in Eq. (13). Then, using Eqs. (12) and (21)–(22) can be expressed as

$$\$_{t,e_2} - \$_{t,e_1} = \sum_{j=1}^{C_{o_1^2}} \dot{q}_{a,o_1^2,j} \hat{\$}_{ta_{o_1,j}} + \sum_{j=1}^{C_{o_2^3}} \dot{q}_{a,o_2^3,j} \hat{\$}_{ta_{o_1,j^*}} + \sum_{j=1}^{6-C_{o_1}} \dot{q}_{c,o_1,j} \hat{\$}_{tc_{o_1,j}} \tag{23}$$

Alternatively, inserting Eqs. (15) and (16) into Eq. (19) gives

$$\begin{aligned}\$_{t,e_2} - \$_{t,e_1} = {} & \sum_{j=1}^{C_{o_1^2}} \dot{q}_{a,o_1^2,j} \hat{\$}_{ta_{o_1,j}} + \sum_{j=1}^{C_{o_2^3}} \dot{q}_{c_s,o_1^2,j} \hat{\$}_{ta_{o_1,j^*}} + \sum_{j=1}^{6-C_{o_1}} \dot{q}_{c_m,o_1^2,j} \hat{\$}_{tc_{o_1,j}} + \sum_{j=1}^{C_{o_1^2}} \dot{q}_{c_s,o_2^3,j} \hat{\$}_{ta_{o_1,j}} + \sum_{j=1}^{C_{o_2^3}} \dot{q}_{a,o_2^3} \hat{\$}_{ta_{o_1,j^*}} \\ & + \sum_{j=1}^{6-C_{o_1}} \dot{q}_{c_m,o_2^3,j} \hat{\$}_{tc_{o_1,j}}\end{aligned} \tag{24}$$

Using the methodology presented by Huang et al. [23], for each unit twist of permission a unit wrench of actuation can be defined which only does work on the considered twist of permission, but that is reciprocal to all other unit twists. Left-multiplication of Eq. (23) with the transposed unit wrenches of actuation associated to the first $C_{o_1^2}$ unit twists $\hat{\$}_{ta_{o_1,j}}$ leads to

$$\mathbf{J}_{a,o_1^2}^{-1}(\$_{t,e_2} - \$_{t,e_1}) = \dot{\boldsymbol{q}}_{a,o_1^2} \tag{25}$$

where

$$\mathbf{J}_{a,o_1^2}^{-1} = \begin{bmatrix} \hat{\$}_{wa_{o_1,1}}^{\mathsf{T}} / (\hat{\$}_{wa_{o_1,1}}^{\mathsf{T}} \hat{\$}_{ta_{o_1,1}}) \\ \hat{\$}_{wa_{o_1,2}}^{\mathsf{T}} / (\hat{\$}_{wa_{o_1,2}}^{\mathsf{T}} \hat{\$}_{ta_{o_1,2}}) \\ \vdots \\ \hat{\$}_{wa_{o_1,C_{o_1^2}}}^{\mathsf{T}} / (\hat{\$}_{wa_{o_1,C_{o_1^2}}}^{\mathsf{T}} \hat{\$}_{ta_{o_1,C_{o_1^2}}}) \end{bmatrix} \tag{26}$$

while left-multiplication of Eq. (24) with the same transposed wrenches results in

$$\mathbf{J}_{a,o_1^2}^{-1}(\$_{t,e_2} - \$_{t,e_1}) = \dot{\boldsymbol{q}}_{a,o_1^2} + \dot{\boldsymbol{q}}_{c_s,o_2^3} \tag{27}$$

where $\mathbf{J}_{a,o_1^2}^{-1}$ was defined in Eq. (26). Eqs. (25) and (27) can be combined into

$$\dot{\boldsymbol{q}}_{c_s,o_2^3} = \boldsymbol{0} \tag{28}$$

which confirms that a motion that is kinematically allowed by the internal serial chain connecting n_1 and n_2, will have zero magnitude in the internal serial chain connecting n_2 and n_3, in which this motion is constrained.

Similarly, left-multiplication of Eq. (23) with the transposed unit wrenches of actuation associated to the last $C_{o_2^3}$ twists of permission of the first end-effector serial chain leads to

$$\mathbf{J}_{a,o_2^3}^{-1}(\$_{t,e_2} - \$_{t,e_1}) = \dot{\boldsymbol{q}}_{a,o_2^3} \tag{29}$$

where

$$\mathbf{J}^{-1}_{a,o_2^3} = \begin{bmatrix} \hat{\$}^{\top}_{wa_{o_{1,1+C_{o_1^2}}}} / (\hat{\$}^{\top}_{wa_{o_{1,1+C_{o_1^2}}}} \hat{\$}_{ta_{o_{1,1+C_{o_1^2}}}}) \\ \hat{\$}^{\top}_{wa_{o_{1,2+C_{o_1^2}}}} / (\hat{\$}^{\top}_{wa_{o_{1,2+C_{o_1^2}}}} \hat{\$}_{ta_{o_{1,2+C_{o_1^2}}}}) \\ \vdots \\ \hat{\$}^{\top}_{wa_{o_{1,C_{o_1}}}} / (\hat{\$}^{\top}_{wa_{o_{1,C_{o_1}}}} \hat{\$}_{ta_{o_{1,C_{o_1}}}}) \end{bmatrix} \tag{30}$$

and left-multiplication of Eq. (24) with those same twists gives

$$\mathbf{J}^{-1}_{a,o_2^3}(\$_{t,e_2} - \$_{t,e_1}) = \dot{\boldsymbol{q}}_{c_s,o_1^2} + \dot{\boldsymbol{q}}_{a,o_2^3} \tag{31}$$

where $\mathbf{J}^{-1}_{a,o_2^3}$ was defined in Eq. (30). Eqs. (29) and (31) can then be combined into

$$\dot{\boldsymbol{q}}_{c_s,o_1^2} = \boldsymbol{0} \tag{32}$$

which confirms that the magnitude of the constrained motion in the internal serial chain connecting n_1 and n_2 is zero for those motions that are kinematically allowed by the internal serial chain connecting n_2 and n_3.

Thus, $\dot{\boldsymbol{q}}_{c_s,o_1^2} = \boldsymbol{0}$, $\dot{\boldsymbol{q}}_{c_s,o_2^3} = \boldsymbol{0}$, and Eqs. (25) and (29) respectively express $\dot{\boldsymbol{q}}_{a,o_1^2}$ and $\dot{\boldsymbol{q}}_{a,o_2^3}$ as a function of the two end-effector twists and the kinematics captured by partial Jacobian matrices. What remains in order to define $\dot{\boldsymbol{q}}_{o_1^2}$ and $\dot{\boldsymbol{q}}_{o_2^3}$ as in Eq. (14), is to derive expressions for $\dot{\boldsymbol{q}}_{c_m,o_1^2}$ and $\dot{\boldsymbol{q}}_{c_m,o_2^3}$.

4.2. Expression for multiple constrained joint velocities in the first end-effector serial chain

Unfortunately, the multiple constrained joint velocities, $\boldsymbol{q}_{c_m,o_1^2}$ and $\boldsymbol{q}_{c_m,o_2^3}$ as part of Eq. (14), cannot be expressed directly as a function of unit twists and unit wrenches. This becomes clear when the result of left-multiplying Eq. (23) with the $6 - C_{o_1}$ unit wrenches of constraint of the first end-effector serial chain is compared with the result of left-multiplying Eq. (24) with those same unit wrenches. Left-multiplication of Eq. (23) with these unit wrenches of constraint gives

$$\mathbf{J}^{-1}_{c,o_1}(\$_{t,e_2} - \$_{t,e_1}) = \dot{\boldsymbol{q}}_{c,o_1} \tag{33}$$

where

$$\mathbf{J}^{-1}_{c,o_1} = \begin{bmatrix} \hat{\$}^{\top}_{wc_{o_{1,1}}} / (\hat{\$}^{\top}_{wc_{o_{1,1}}} \hat{\$}_{tc_{o_{1,1}}}) \\ \hat{\$}^{\top}_{wc_{o_{1,2}}} / (\hat{\$}^{\top}_{wc_{o_{1,2}}} \hat{\$}_{tc_{o_{1,2}}}) \\ \vdots \\ \hat{\$}^{\top}_{wc_{o_{1,6-C_{o_1}}}} / (\hat{\$}^{\top}_{wc_{o_{1,6-C_{o_1}}}} \hat{\$}_{tc_{o_{1,6-C_{o_1}}}}) \end{bmatrix} \tag{34}$$

On the other hand, left-multiplying Eq. (24) with the same unit wrenches of constraint gives

$$\mathbf{J}^{-1}_{c,o_1}(\$_{t,e_2} - \$_{t,e_1}) = \dot{\boldsymbol{q}}_{c_m,o_1^2} + \dot{\boldsymbol{q}}_{c_m,o_2^3} \tag{35}$$

Eqs. (33) and (35) can be combined into

$$\dot{\boldsymbol{q}}_{c_m,o_1^2} + \dot{\boldsymbol{q}}_{c_m,o_2^3} = \dot{\boldsymbol{q}}_{c,o_1} \tag{36}$$

where $\dot{\boldsymbol{q}}_{c,o_1}$ is defined by Eq. (33). Eq. (36) cannot be solved for $\dot{\boldsymbol{q}}_{c_m,o_1^2}$ and $\dot{\boldsymbol{q}}_{c_m,o_2^3}$ directly.

To obtain a closed form expression for $\dot{\boldsymbol{q}}_{c_m,o_1^2}$ and $\dot{\boldsymbol{q}}_{c_m,o_2^3}$, Eq. (36) is complemented with an additional set of equations, which are based on static force relations. For each node of the PM2E it holds that in a static equilibrium the sum of all wrenches is zero. In a quasi-static equilibrium, also the derivative with respect to time of this sum is zero, and for body n_2 it holds that

$$\frac{d\$_{w,2}}{dt} + \frac{d\$_{w,o_1^2}}{dt} - \frac{d\$_{w,o_2^3}}{dt} = 0 \tag{37}$$

In order to complement Eq. (36), only the motions that are multiple constrained by the internal serial chains are of interest. To simplify the further derivation, it is assumed that the change in wrenches is dominated by stiffness and that along those directions the stiffness of the second leg is significantly less than the stiffness of the internal serial chains. Then, the term $d\$_{w,2}/dt$ in Eq. (37) can be neglected for those directions. Next, because the two internal serial chains share the same joint coordinates, Eq. (37) can be also expressed in those multiple constrained joint coordinates, so that

$$\mathbf{K}_{q_{c_m,o_1^2}} \dot{\boldsymbol{q}}_{c_m,o_1^2} - \mathbf{K}_{q_{c_m,o_2^3}} \dot{\boldsymbol{q}}_{c_m,o_2^3} = 0 \tag{38}$$

where $\mathbf{K}_{q_{c_m,o_1^2}}$ is the stiffness matrix of the internal chain connecting n_1 to n_2 and $\mathbf{K}_{q_{c_m,o_2^3}}$ is the stiffness matrix of the internal chain connecting n_2 to n_3, both expressed in the multiple constrained joint space of the first end-effector serial chain.

Eqs. (36) and (38) can be combined into

$$\begin{bmatrix} \mathbf{I}_{(6-C_{o_1})} & \mathbf{I}_{(6-C_{o_1})} \\ \mathbf{K}_{q_{c_m,o_1^2}} & -\mathbf{K}_{q_{c_m,o_2^3}} \end{bmatrix} \begin{bmatrix} \dot{\boldsymbol{q}}_{c_m,o_1^2} \\ \dot{\boldsymbol{q}}_{c_m,o_2^3} \end{bmatrix} = \begin{bmatrix} \mathbf{I}_{(6-C_{o_1})} \\ \mathbf{0}_{(6-C_{o_1})} \end{bmatrix} \dot{\boldsymbol{q}}_{c,o_1} \tag{39}$$

in which the identity matrix $\mathbf{I}_{(6-C_{o_1})}$, and the stiffness matrices $\mathbf{K}_{q_{c_m,o_1^2}}$ and $\mathbf{K}_{q_{c_m,o_2^3}}$ are all of size $(6 - C_{o_1}) \times (6 - C_{o_1})$. Eq. (39) can be written as

$$\begin{bmatrix} \dot{\boldsymbol{q}}_{c_m,o_1^2} \\ \dot{\boldsymbol{q}}_{c_m,o_2^3} \end{bmatrix} = \begin{bmatrix} \mathbf{I}_{(6-C_{o_1})} & \mathbf{I}_{(6-C_{o_1})} \\ \mathbf{K}_{q_{c_m,o_1^2}} & -\mathbf{K}_{q_{c_m,o_2^3}} \end{bmatrix}^{-1} \begin{bmatrix} \mathbf{I}_{(6-C_{o_1})} \\ \mathbf{0}_{(6-C_{o_1})} \end{bmatrix} \dot{\boldsymbol{q}}_{c,o_1} \tag{40}$$

which can be developed using matrix inversion rules into

$$\begin{bmatrix} \dot{\boldsymbol{q}}_{c_m,o_1^2} \\ \dot{\boldsymbol{q}}_{c_m,o_2^3} \end{bmatrix} = \begin{bmatrix} \mathbf{K}^{-1}_{q_{c_m,o_1^2}} \left(\mathbf{K}^{-1}_{q_{c_m,o_1^2}} + \mathbf{K}^{-1}_{q_{c_m,o_2^3}} \right)^{-1} \\ \mathbf{K}^{-1}_{q_{c_m,o_2^3}} \left(\mathbf{K}^{-1}_{q_{c_m,o_1^2}} + \mathbf{K}^{-1}_{q_{c_m,o_2^3}} \right)^{-1} \end{bmatrix} \dot{\boldsymbol{q}}_{c,o_1} \tag{41}$$

where $\dot{\boldsymbol{q}}_{c,o_1}$ was expressed in Eq. (33) as function of the two end-effector twists. As such, Eq. (41) expresses $\dot{\boldsymbol{q}}_{c_m,o_1^2}$ and $\dot{\boldsymbol{q}}_{c_m,o_2^3}$ as a function of the two end-effector twists and the relative compliance of the two respective internal serial chains.

4.3. Internal mapping of twists

Eqs. (25), (27), (29), (32) and (41) have expressed all joint velocities of the two internal serial chains that make up the first end-effector serial chain as a function of the two end-effector twists. Then, forward Jacobian mapping can be used to express the twist of n_2 as a function of the two end-effector twists. There are two equivalent options to do so, namely those introduced in Eqs. (9) and (10). In this paper the representation in Eq. (9) is chosen, but it should be noted that this is an arbitrary choice and does not affect the results.

The twist of the first internal serial chain was expressed as the sum of six unit twists in Eq. (15), which can also be expressed in matrix form as

$$\$_{t,o_1^2} = \begin{bmatrix} \mathbf{J}_{a,o_1^2} & \mathbf{J}_{a,o_2^3} & \mathbf{J}_{c,o_1} \end{bmatrix} \begin{bmatrix} \dot{\boldsymbol{q}}_{a,o_1^2} \\ \dot{\boldsymbol{q}}_{c_s,o_1^2} \\ \dot{\boldsymbol{q}}_{c_m,o_1^2} \end{bmatrix} \tag{42}$$

where

$$\mathbf{J}_{a,o_1^2} = \begin{bmatrix} \hat{\$}_{ta_{o_1,1}} & \hat{\$}_{ta_{o_1,2}} & \cdots & \hat{\$}_{ta_{o_1,C_{o_1^2}}} \end{bmatrix} \tag{43}$$

$$\mathbf{J}_{a,o_2^3} = \begin{bmatrix} \hat{\$}_{ta_{o_1,1+C_{o_1^2}}} & \hat{\$}_{ta_{o_1,2+C_{o_1^2}}} & \cdots & \hat{\$}_{ta_{o_1,C_{o_1}}} \end{bmatrix} \tag{44}$$

$$\mathbf{J}_{c,o_1} = \begin{bmatrix} \hat{\$}_{tc_{o_1,1}} & \hat{\$}_{tc_{o_1,2}} & \cdots & \hat{\$}_{tc_{o_1,(6-C_{o_1})}} \end{bmatrix} \tag{45}$$

Then, using the part of Eq. (41) that expresses $\dot{\boldsymbol{q}}_{c_m,o_1^2}$, Eq. (42) can be rewritten as

$$\$_{t,o_1^2} = \begin{bmatrix} \mathbf{J}_{a,o_1^2} & \mathbf{J}_{a,o_2^3} & \mathbf{J}_{c,o_1} \end{bmatrix} \begin{bmatrix} \dot{\boldsymbol{q}}_{a,o_1^2} \\ \dot{\boldsymbol{q}}_{c_s,o_1^2} \\ \mathbf{M}_{q_{c_m,o_1^2}} \dot{\boldsymbol{q}}_{c,o_1} \end{bmatrix} \tag{46}$$

in which

$$\mathbf{M}_{q_{c_m,o_1^2}} = \mathbf{K}^{-1}_{q_{c_m,o_1^2}} \left(\mathbf{K}^{-1}_{q_{c_m,o_1^2}} + \mathbf{K}^{-1}_{q_{c_m,o_2^3}} \right)^{-1} \tag{47}$$

Next, the expressions for $\dot{\boldsymbol{q}}_{a,o_1^2}$ and $\dot{\boldsymbol{q}}_{c,o_1}$ as introduced in Eqs. (25) and (33), and the relation $\dot{\boldsymbol{q}}_{c_s,o_1^2} = \boldsymbol{0}$ as introduced in Eq. (32), allows Eq. (46) to be written as

$$\$_{t,o_1^2} = (\mathbf{M}_{a,o_1^2} + \mathbf{M}_{c,o_1^2})(\$_{t_{e_2}} - \$_{t_{e_1}}) \tag{48}$$

where

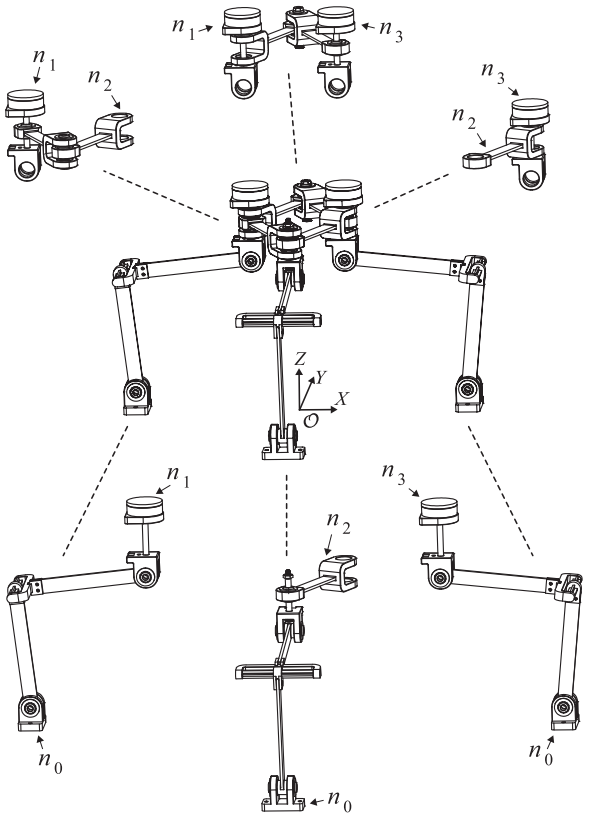

Fig. 4. The example Jacobian analysis was performed for a 2-DoF PM2E where the second joint of each leg was designed as a compliant joint.

$$\mathbf{M}_{a,o_1^2} = \mathbf{J}_{a,o_1^2}\mathbf{J}^{-1}_{a,o_1^2} \tag{49}$$

$$\mathbf{M}_{c,o_1^2} = \mathbf{J}_{c,o1}\mathbf{M}_{q_{cm},o_1^2}\mathbf{J}^{-1}_{c,o1} \tag{50}$$

Finally, Eqs. (48) and (8) can be inserted in Eq. (9), such that $\mathbf{M}_t$ in Eq. (7) is developed as

$$\mathbf{M}_t = \begin{bmatrix} \mathbf{I} & \mathbf{0} \\ (\mathbf{I} - \mathbf{M}_{a,o_1^2} - \mathbf{M}_{c,o_1^2}) & (\mathbf{M}_{a,o_1^2} + \mathbf{M}_{c,o_1^2}) \\ \mathbf{0} & \mathbf{I} \end{bmatrix} \tag{51}$$

where all matrices on the right side of the equal sign are 6×6 matrices. Eq. (51) maps the two end-effector twists onto the three terminal link twists, which can be subsequently mapped onto the complete set of joint velocities as in Eq. (5).

5. Example jacobian analysis of a three-legged PM2E

In this section the inverse Jacobian analysis is performed for the three-legged 2-DoF PM2E shown in Fig. 4, where n_1 and n_3 are considered as the end-effectors. The architecture of this PM2E was introduced as part of the kinematic design exercise in Ref. [24] and is also represented in Fig. 3c. The PM2E has two DoFs, as described in Ref. [24]. The first DoF is a motion along the Z-axis, shared by both end-effectors, and the second DoF is a relative motion between the end-effectors along the X-axis, i.e., gripping. For the purpose of experimental validation, the end-effectors are connected to wrench sensors, which measure both force and moment. Additionally, the second joint of each leg is realized using a compliant joint, so that a pose-dependent wrench is applied on both end-effectors without the need of an actuation system. All other joints are realized using ball-bearings and are therefore considered as zero stiffness joints.

The inverse Jacobian matrix $\mathbf{J}^{-1}$, introduced in Eq. (6), for a three-legged PM2E with an internal closed-loop chain is obtained by combining the results from Sections 3 and 4. Then,

$$\begin{bmatrix} \dot{\boldsymbol{q}}_1 \\ \dot{\boldsymbol{q}}_2 \\ \dot{\boldsymbol{q}}_3 \\ \dot{\boldsymbol{q}}_{o_1^2} \\ \dot{\boldsymbol{q}}_{o_2^3} \\ \dot{\boldsymbol{q}}_{o_3^1} \end{bmatrix} = \mathbf{J}^{-1} \begin{bmatrix} \$_{t,e_1} \\ \$_{t,e_2} \end{bmatrix} \tag{52}$$

with

$$\mathbf{J}^{-1} = \mathbf{J}_n^{-1} \mathbf{M}_t \tag{53}$$

where the matrix $\mathbf{M}_t$ was introduced in Eq. (51) and for a three-legged PM2E with one internal closed-loop chain $\mathbf{J}_n^{-1}$ in Eq. (53) is developed as in Eq. (6), namely

$$\mathbf{J}_n^{-1} = \begin{bmatrix} \mathbf{J}_1^{-1} & \mathbf{0}_{6\times6} & \mathbf{0}_{6\times6} \\ \mathbf{0}_{6\times6} & \mathbf{J}_2^{-1} & \mathbf{0}_{6\times6} \\ \mathbf{0}_{6\times6} & \mathbf{0}_{6\times6} & \mathbf{J}_3^{-1} \\ -\mathbf{J}_{o_1^2}^{-1} & \mathbf{J}_{o_1^2}^{-1} & \mathbf{0}_{6\times6} \\ \mathbf{0}_{6\times6} & -\mathbf{J}_{o_2^3}^{-1} & \mathbf{J}_{o_2^3}^{-1} \\ \mathbf{J}_{o_3^1}^{-1} & \mathbf{0}_{6\times6} & -\mathbf{J}_{o_3^1}^{-1} \end{bmatrix} \tag{54}$$

The partial inverse Jacobian matrices in Eq. (54) are introduced in Appendix A, where they are expressed using the unit twists and unit wrenches for each serial chain. As explained in Section 4, the unit twists and unit wrenches that are identified for the two end-effector serial chains are also used in the analysis of the three internal serial chains, because they share the same kinematic structures.

To develop the matrix $\mathbf{M}_t$, which maps the end-effector twists on the full set of terminal link twists, $\mathbf{M}_{a,o_1^2}$ and $\mathbf{M}_{c,o_1^2}$ need to be developed. Because $C_{o_1^2} = 2$, the matrix $\mathbf{M}_{a,o_1^2}$ is obtained using Eq. (49), in which $\mathbf{J}_{a,o_1^2}$ is expressed by Eq. (43) as

$$\mathbf{J}_{a,o_1^2} = \begin{bmatrix} \hat{\$}_{ta_{o_{1,1}}} & \hat{\$}_{ta_{o_{1,2}}} \end{bmatrix} \tag{55}$$

and $\mathbf{J}_{a,o_1^2}^{-1}$ is expressed by Eq. (26) as

$$\mathbf{J}_{a,o_1^2}^{-1} = \begin{bmatrix} \hat{\$}_{wa_{o_{1,1}}}^{\top} / (\hat{\$}_{wa_{o_{1,1}}}^{\top} \hat{\$}_{ta_{o_{1,1}}}) \\ \hat{\$}_{wa_{o_{1,2}}}^{\top} / (\hat{\$}_{wa_{o_{1,2}}}^{\top} \hat{\$}_{ta_{o_{1,2}}}) \end{bmatrix} \tag{56}$$

The matrix $\mathbf{M}_{c,o_1^2}$ is constructed from three matrices: $\mathbf{J}_{c,o_1}$, $\mathbf{J}_{c,o_1}^{-1}$, and $\mathbf{M}_{q_{c_m,o_1^2}}$, as expressed in Eq. (50). Because $C_{o_1} = 3$, it follows from Eqs. (45) and (34) that

$$\mathbf{J}_{c,o_1} = \begin{bmatrix} \hat{\$}_{tc_{o_{1,1}}} & \hat{\$}_{tc_{o_{1,2}}} & \hat{\$}_{tc_{o_{1,3}}} \end{bmatrix} \tag{57}$$

$$\mathbf{J}_{c,o_1}^{-1} = \begin{bmatrix} \hat{\$}_{wc_{o_{1,1}}}^{\top} / (\hat{\$}_{wc_{o_{1,1}}}^{\top} \hat{\$}_{tc_{o_{1,1}}}) \\ \hat{\$}_{wc_{o_{1,2}}}^{\top} / (\hat{\$}_{wc_{o_{1,2}}}^{\top} \hat{\$}_{tc_{o_{1,2}}}) \\ \hat{\$}_{wc_{o_{1,3}}}^{\top} / (\hat{\$}_{wc_{o_{1,3}}}^{\top} \hat{\$}_{tc_{o_{1,3}}}) \end{bmatrix} \tag{58}$$

To express $\mathbf{M}_{q_{c_m,o_1^2}}$ using Eq. (47), the compliance matrices $\mathbf{K}_{q_{c_m,o_1^2}}^{-1}$ and $\mathbf{K}_{q_{c_m,o_2^3}}$ are required, which are the compliance matrices of the internal serial chains expressed in the multiple constrained joint space, which is spanned by the twists associated to the virtual joints of the first end-effector serial chain. The compliance in these directions is assumed to originate solely in the links. Each internal serial chain contains one link, each of which was designed as a rectangular bar. The required compliance matrices are therefore developed by mapping the relevant link compliance matrix onto the constrained joint space of the first end-effector serial chain,

$$\mathbf{K}_{q_{c_m,o_1^2}}^{-1} = \mathbf{J}_{c,o_1}^{-1} \mathbf{Ad}_{\mathbf{H}_{l_{o_{1,1}}}^{\mathcal{O}}} \mathbf{K}_{s,l_{o_{1,1}}}^{-1} \mathbf{Ad}_{\mathbf{H}_{l_{o_{1,1}}}^{\mathcal{O}}}^{\top} \mathbf{J}_{c,o_1}^{-\top} \tag{59}$$

$$\mathbf{K}_{q_{c_m,o_2^3}}^{-1} = \mathbf{J}_{c,o_1}^{-1} \mathbf{Ad}_{\mathbf{H}_{l_{o_{1,2}}}^{\mathcal{O}}} \mathbf{K}_{s,l_{o_{1,2}}}^{-1} \mathbf{Ad}_{\mathbf{H}_{l_{o_{1,2}}}^{\mathcal{O}}}^{\top} \mathbf{J}_{c,o_1}^{-\top} \tag{60}$$

where $\mathbf{J}_{c,o_1}^{-1}$ was introduced in Eq. (58), and $\mathbf{Ad}_{\mathbf{H}_{l_{o_{1,i}}}^{\mathcal{O}}}$ is the Adjoint matrix which transforms a twist expressed in the reference frame connected to the end of the i th link of the first end-effector serial chain into its equivalent twist expressed in the inertial Cartesian

reference frame, and $\mathbf{K}^{-1}_{s,l_{o1,i}}$ is the compliance matrix of the i th link of the first end-effector serial chain. Both links were designed equal, such that

$$\mathbf{K}^{-1}_{s,l_{o1,i}} = \begin{bmatrix} \frac{L_o}{GI_x} & 0 & 0 & 0 & 0 & 0 \\ 0 & \frac{L_o}{EI_y} & 0 & 0 & 0 & \frac{-L_o^2}{2EI_y} \\ 0 & 0 & \frac{L_o}{EI_z} & 0 & \frac{L_o^2}{2EI_z} & 0 \\ 0 & 0 & 0 & \frac{L_o}{AE} & 0 & 0 \\ 0 & 0 & \frac{L_o^2}{2EI_z} & 0 & \frac{L_o^3}{3EI_z} & 0 \\ 0 & -\frac{L_o^2}{2EI_y} & 0 & 0 & 0 & \frac{L_o^3}{3EI_y} \end{bmatrix} \tag{61}$$

For the developed mechanism, $L_o = 0.12$ m, $E = 1.95{\cdot}10^9$ N/m^2, and $G = 740{\cdot}10^6$ N/m^2 was subsequently calculated using

$$G = E/(2 + 2\nu) \tag{62}$$

with $\nu = 0.32$, where E and ν were determined as the average values of two tensile tests, which were performed on samples of the material used for the construction of the links, namely Stratasys ABS plus material in combination with a Stratasys Dimension BST 1200es 3D printer. Individual determined values for E had a 4% difference from this value. Furthermore, the area and the area moments of inertia, respectively, are

$$A = bh \quad I_x = 1/12bh\,(h^2 + b^2), \quad I_y = 1/12bh^3, \quad I_z = 1/12b^3h$$

with $b = 3$ mm and $h = 16$ mm.

With the matrices introduced in Eqs. (55)–(61), the matrices $\mathbf{M}_{a,o_1^2}$ and $\mathbf{M}_{c,o_1^2}$ are developed according to Eqs. (49) and (50). Subsequently, $\mathbf{M}_t$ was developed using Eq. (51) and $\mathbf{J}_n^{-1}$ was constructed as in Eq. (54) using the partial inverse Jacobian matrices developed in Appendix A. Finally, the complete inverse Jacobian matrix of the PM2E presented in Fig. 4 was obtained using Eq. (53).

6. Experimental validation method

To validate the developed Jacobian analysis, an experimental static force analysis was performed for the PM2E introduced in Section 5. The reason for using a static force analysis is because it is relatively easy to control the pose, which determines the torques applied by the compliant joints, and measure the resulting six-dimensional reaction wrenches at both end-effectors. On the other hand, it is considered much more difficult to simultaneously control the end-effector twists and measure the complete set of joint velocities. This is especially true for the constrained directions.

6.1. Static force analysis

In a static force analysis, the transpose of an inverse Jacobian matrix can be used to map a known joint torque vector onto the equivalent wrenches applied by the end-effector on the environment. Therefore, if the compliant mechanism with two end-effectors as introduced in Fig. 4 is fixed in a specific pose through its end-effectors, the interaction wrenches can be predicted as a function of the pose, namely

$$\begin{bmatrix} \$_{w,e_1} \\ \$_{w,e_2} \end{bmatrix} = \mathbf{J}^{-\top}\boldsymbol{\tau} \tag{63}$$

where $\$_{w,e_1}$ and $\$_{w,e_2}$ are the net wrenches applied by the PM2E on the first and second end-effector respectively, $\mathbf{J}^{-\top}$ is the transpose of the full inverse Jacobian and $\boldsymbol{\tau}$ is the applied joint torque vector, which is expressed as

$$\boldsymbol{\tau} = \begin{bmatrix} \boldsymbol{\tau}_1^\top & \boldsymbol{\tau}_2^\top & \boldsymbol{\tau}_3^\top & \boldsymbol{\tau}_{o_1^2}^\top & \boldsymbol{\tau}_{o_2^3}^\top & \boldsymbol{\tau}_{o_{31}}^\top \end{bmatrix}^\top \tag{64}$$

where $\boldsymbol{\tau}_\mathbf{i}$ is the six-dimensional joint torque vector for leg i, and $\boldsymbol{\tau}_{\mathbf{o_i i+1}}$ (or $\boldsymbol{\tau}_{o_i 1}$ if i=N) is the six-dimensional joint torque vector of the ith internal serial chain.

For the example that was introduced in Section 5, the internal serial chains do not contain any actuated or compliant joints joints. And although constraint forces may be transferred by the internal serial chains, they are not generated by the internal serial chains, so that

$$\boldsymbol{\tau}_{o_1^2} = \boldsymbol{\tau}_{o_2^3} = \boldsymbol{\tau}_{o_3^1} = \mathbf{0}_{6\times1} \tag{65}$$

The only torques generated by the legs are due to the compliant revolute joints, so that

$$\boldsymbol{\tau}_\mathbf{i} = [0 \;\; \tau_{pf,i} \;\; 0 \;\; 0 \;\; 0 \;\; 0]^\top, \quad \text{for} i = 1, 2, 3 \tag{66}$$

Table 1
The 18 poses at which the Jacobian analysis of the example PM2E has been validated using a static force analysis.

Pose	p_{x,e_1} [m]	p_{z,e_1} [m]	p_{x,e_2} [m]	p_{z,e_2} [m]
a0	−0.0525	0.2165	0.0525	0.2165
a1	−0.0575	0.2165	0.0575	0.2165
a2	−0.0525	0.2215	0.0525	0.2215
b0	−0.070	0.2165	0.070	0.2165
b1	−0.075	0.2165	0.075	0.2165
b2	−0.070	0.2215	0.070	0.2215
c0	−0.065	0.200	0.065	0.200
c1	−0.070	0.200	0.070	0.200
c2	−0.065	0.205	0.065	0.205
d0	−0.055	0.205	0.055	0.205
d1	−0.060	0.205	0.060	0.205
d2	−0.055	0.210	0.055	0.210
e0	−0.055	0.190	0.055	0.190
e1	−0.060	0.190	0.060	0.190
e2	−0.055	0.195	0.055	0.195
f0	−0.060	0.220	0.060	0.220
f1	−0.065	0.220	0.065	0.220
f2	−0.060	0.225	0.060	0.225

where $\tau_{pf,i}$ is the joint torque resulting from the deflection of the compliant revolute joint that makes up the second joint of each leg, so that

$$\tau_{pf,i} = -k_i(q_{i,2} - q_{i,2_0}), \quad \text{for} i = 1, 2, 3 \tag{67}$$

To express the stiffness k_i (Nm/rad) of the designed cross-type compliant revolute joint, the model presented by Trease et al. [25] was used, namely

$$k_i = \left(\frac{w}{t} - 0.373\right)\frac{4Gt^4}{3L_j}, \quad \text{for} i = 1, 2, 3 \tag{68}$$

where the designed cross-type compliant joint has width $w = 9$ mm, thickness $t = 2$ mm, length $L_j = 40$ mm, and is made of the same Stratasys ABS plus material as the links in the end-effector serial chains, so that $G = 740{\cdot}10^6$ N/m^2 and $E = 1.95{\cdot}10^9$ N/m^2. The angle of zero deflection, $q_{i,2_0}$ (rad), was designed as

$$q_{i,2_0} = \frac{3\pi}{2} \quad \text{for} i = 1, 2, 3 \tag{69}$$

An expression for the angles $q_{i,2}$ can be found in Appendix B.

6.2. Measurement procedure

The mapping of the applied joint torque vector onto the resulting interaction wrenches was performed in the 18 poses as introduced in Table 1. These reaction wrenches were measured using an ATI Mini40 wrench sensor with SI-40-2 calibration. The specified force measurement accuracy of this sensor along the X- and Y-axis is 1/100 N and 1/50 N along the Z-axis. The torque measurement accuracy is 1/4000 Nm for all three directions. Both wrench sensors were connected in series between one of the end-effectors and the inertial measurement frame, as can be seen in Fig. 5b. As such, the wrench sensors were displaced together with the end-effector bodies. Before the start of every measurement series, the wrench sensor was initialized at the pose where the net wrench on the end-effectors is approximately zero, which is pose a0 as introduced in Table 1. The position of the end-effector within the measurement frame was controlled manually using a caliper. This was done by moving the attachment beams of the two end-effectors in the X- and Z-directions, as shown in Figs. 5b and c, where where arrows indicate how the positions p_{x,e_1}, p_{x,e_2}, p_{z,e_1}, and p_{z,e_2} are changed by adjusting the measurement frame.

There are various sources that may influence the measurement precision and accuracy. Firstly, next to the finite resolution of the wrench sensors, there are inevitable inaccuracies in the manual positioning of the end-effectors. Secondly, the model will not be perfect, because the change in gravity is not considered, nor is any friction in the ball bearings. Furthermore, the 3D-printed compliant joints will likely show some variation in their properties, and therefore not perfectly agree with the modeled joints.

6.3. Post-processing

Post-processing of the data was necessary to express all wrenches in the measurement reference frame of either the first or the second end-effector, so that measured and predicted wrenches could be compared. The wrenches that are expressed using the

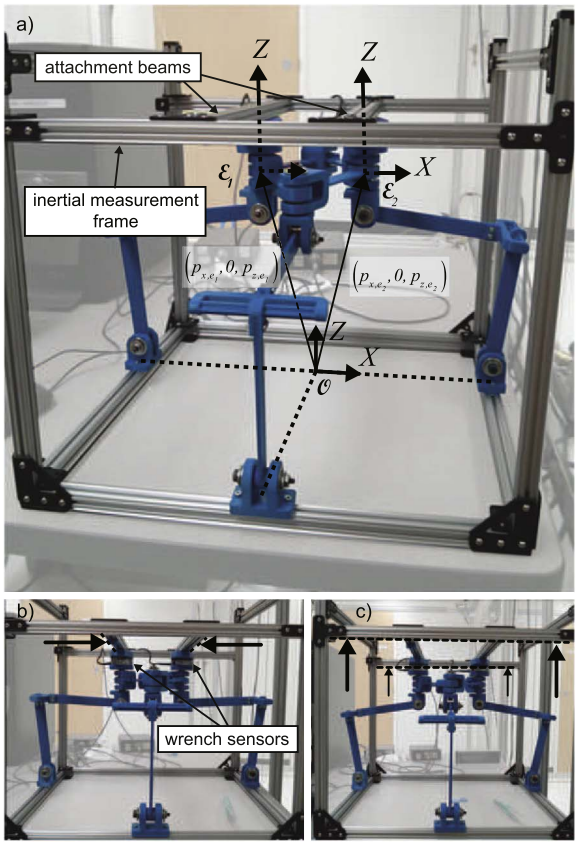

Fig. 5. The set-up used to validate the developed Jacobian analysis, a) in pose a0, in which the net wrench is approximately zero, b) in pose f0, and c) pose f1.

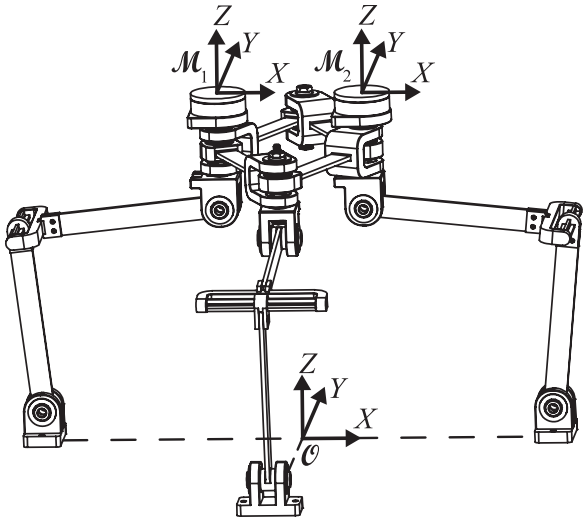

Fig. 6. The inertial reference frame and the measurement reference frames as used in the example Jacobian analysis.

Jacobian-based mapping of the compliant joint torques are all expressed in end-effector body-fixed reference frames collocated with the inertial reference frame. However, the measurements are made in measurement reference frames, as shown in Fig. 6. The mapping of the two predicted interaction wrenches onto the measurement reference frames was done using

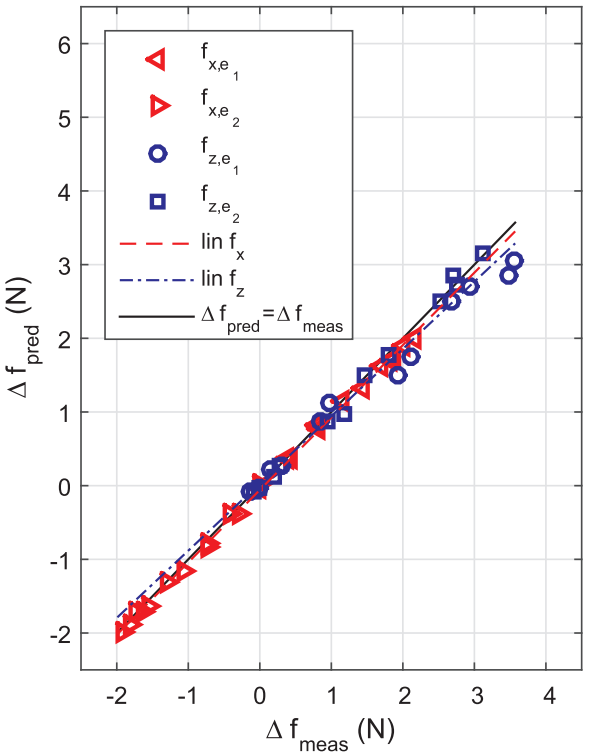

Fig. 7. The correlation between the measured force values and those predicted using $\mathbf{J}^{-\mathsf{T}}$ at the poses as listed in Table 1 along the axes spanned by the DoFs of the PM2E.

$$\begin{bmatrix} \$^{\mathcal{M}_1}_{w,e_1,pred} \\ \$^{\mathcal{M}_2}_{w,e_2,pred} \end{bmatrix} = \begin{bmatrix} \mathbf{Ad}^{\mathsf{T}}_{\mathbf{H}^{O}_{\mathcal{M}_1}} & \mathbf{0}_6 \\ \mathbf{0}_6 & \mathbf{Ad}^{\mathsf{T}}_{\mathbf{H}^{O}_{\mathcal{M}_2}} \end{bmatrix} \begin{bmatrix} \$^{O}_{w,e_1,pred} \\ \$^{O}_{w,e_2,pred} \end{bmatrix} \tag{70}$$

where $\$^{O}_{w,e_1,pred}$ and $\$^{O}_{w,e_2,pred}$ are the predicted interaction wrenches expressed in the inertial reference frame and $\$^{\mathcal{M}_1}_{w,e_1,pred}$ and $\$^{\mathcal{M}_2}_{w,e_2,pred}$ are the equivalent wrenches expressed in their respective measurement frames. Matrices $\mathbf{Ad}_{\mathbf{H}^{O}_{\mathcal{M}_1}}$ and $\mathbf{Ad}_{\mathbf{H}^{O}_{\mathcal{M}_2}}$ are the adjoint matrices associated to the homogeneous matrices $\mathbf{H}^{O}_{\mathcal{M}_1}$ and $\mathbf{H}^{O}_{\mathcal{M}_2}$. These homogeneous matrices were expressed as

$$\mathbf{H}^{O}_{\mathcal{M}_1} = \begin{bmatrix} \mathbf{I}_3 & \boldsymbol{p}_{m_1} \\ \mathbf{0}_{1\times 3} & 1 \end{bmatrix} \mathbf{H}^{O}_{\mathcal{M}_2} = \begin{bmatrix} \mathbf{I}_3 & \boldsymbol{p}_{m_2} \\ \mathbf{0}_{1\times 3} & 1 \end{bmatrix}$$

with

$$\boldsymbol{p}_{m_1} = [p_{x,e_1} \;\; 0 \;\; p_{z,e_1} + h_s]^{\mathsf{T}} \boldsymbol{p}_{m_2} = [p_{x,e_2} \;\; 0 \;\; p_{z,e_2} + h_s]^{\mathsf{T}}$$

where h_s=42.6 [mm] was the distance between the end-effector reference frame origins, as shown in Fig. 5, and the measurement reference frames, as shown in Fig. 6. After mapping as in Eq. (70), the wrenches predicted by Jacobian mapping can be compared with those measured.

7. Results

This section presents the results of the experimental validation as described in Section 6. The results are visualized in Figs. 7–9. Fig. 7 plots the predicted interaction force values against those measured for the *X*- and *Z*-axis, which are the axes spanned by the DoFs of the analyzed PM2E. In Fig. 7, the individual measurement are organized by axis as well as by end-effector. Additionally, linear trend lines are shown for the complete set of measured forces along both the *X*- and *Z*-axis.

In Fig. 8 a similar plot is shown for the *Y*-axis, which represents a constraint of the PM2E for both end-effectors. Finally, the predicted and measured interaction moments are plotted against each other in Fig. 9, where the example PM2E is constrained in rotational motion along all three axes. The complete set of measurement data can be obtained from Ref. [26].

To express the percentage of variability in the measurements that has been accounted for by the Jacobian-based predictions, the coefficients of determination, R^2, are used. These coefficients are shown in Table 2 for the data shown in Figs. 7–9. The R^2 values

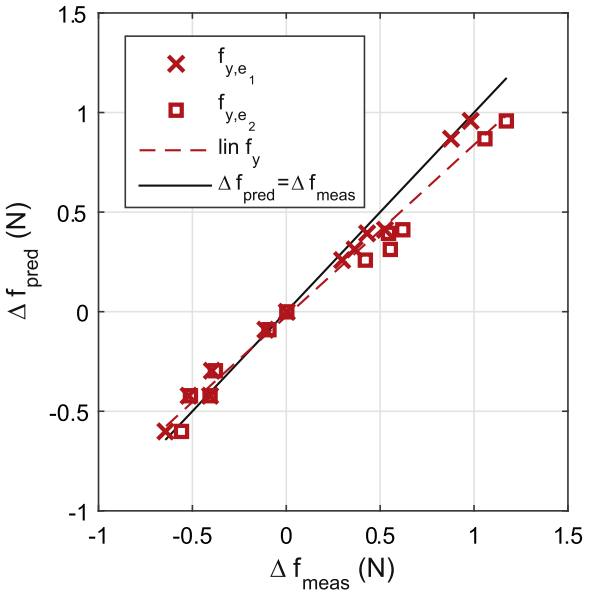

Fig. 8. The correlation between the measured force values and those predicted using $\mathbf{J}^{-\mathrm{T}}$ at the poses listed in Table 1 along the axis in which the PM2E is constrained.

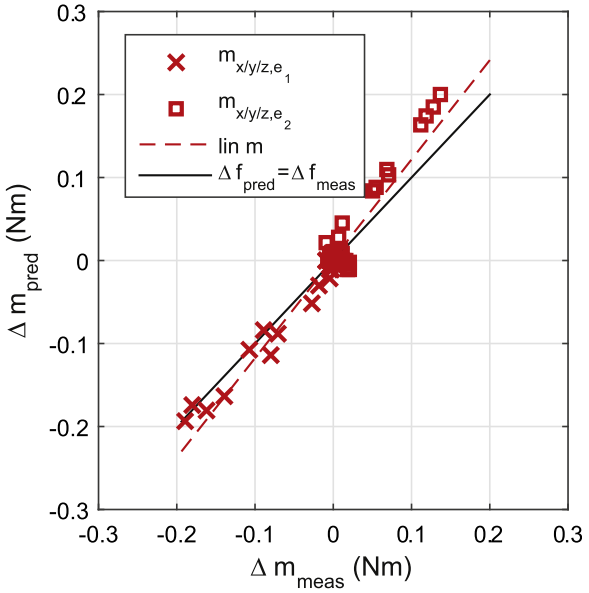

Fig. 9. The correlation between the measured moment values and those predicted using $\mathbf{J}^{-\mathrm{T}}$ at the poses listed in Table 1 along all three axes, all of which are constrained directions for the analyzed PM2E.

express the variability around the linear trend lines which are included in Figs. 7–9. Also, for comparison, the ideal linear trend lines, namely $\Delta f_{pred} = \Delta f_{meas}$ are also shown.

8. Discussion

The results from the experimental validation of the Jacobian analysis demonstrate that the presented Jacobian analysis is valid for the analyzed three-legged PM2E with a single internal closed-loop chain. This is concluded from the high coefficients of determination for the three separately analyzed sets of predicted and measured force and moment values, as presented in Table 2. Although the coefficient of determination for the angular constraints is somewhat lower, this can be explained by the large number of values close to zero, which are more affected by measurement errors. Nonetheless, these values are considered sufficiently high to

Table 2
The coefficients of determination of the different sets of measured and predicted values.

considered set	related figure	R^2 [-]
DoFs ($f_{x/z}$)	Fig. 7	0.996
linear constraints (f_y)	Fig. 8	0.962
angular constraints ($\boldsymbol{m}_{x/y/z}$)	Fig. 9	0.876

conclude that the Jacobian analysis that was used to predict the interaction wrenches is valid.

Although the presented Jacobian analysis was developed based on velocity relations, it was validated using a static force analysis for three reasons. Firstly, it was considered more practical to control the pose during static wrench measurements than during velocity measurements. Secondly, it was deemed much simpler to include the constraints in static force measurements than in velocity measurements. The third reason is that constraint relations are especially important in the static force analysis of PM2Es, since wrenches applied by the legs can be transferred via the constraints of internal serial chains. The inclusion of these constraint relations in the matrix $\mathbf{M}_t$, which represents the mapping from the two end-effector twists onto the full set of terminal link twists, has been one of the main innovations of this paper. Therefore, a static force analysis has allowed a direct validation of this innovation.

It is argued that the example PM2E is a representative example of more general PM2Es with an internal closed-loop chain. The main difficulty of the analysis was to find an expression for the mapping from the two end-effector twists onto the complete set of terminal link twists. A combination of velocity relations and static force relations was derived to deal with the internal constraints. As a result, the obtained expression is a function of the kinematic structure of the mechanism as well as the relative compliance of the internal serial chains. The proposed systematic approach can be extended to PM2Es with an internal closed-loop chain with more than three legs, knowing that more, comparable relations will need to be expressed to reflect its corresponding graph representation.

Furthermore, it is expected that the presented systematic approach can be easily adapted to other variations of PM2Es. Because the analysis relies on a Jacobian interpretation of a PM's graph theory representation, the same approach can also be applied to other, more complex parallel manipulators, e.g., with more than one internal closed-loop chain or with more than two end-effectors. Such manipulators will have different graph theory representations, which means that the structures of the corresponding matrices $\mathbf{J}_n^{-1}$ would be different than the one presented in Eq. (6). Nonetheless, the approach would be the same. As such, the systematic approach presented in this paper could be used as a baseline for a wide range of more complex parallel manipulators.

9. Conclusions

This paper introduced a systematic approach for the Jacobian analysis of PM2Es with an internal closed-loop chain, based on two novel insights. The first insight is that the structure that is revealed by graph theory can be translated into a Jacobian analysis. The resulting Jacobian analysis consists of a systematic combination of partial Jacobian matrices, which describes how the full set of terminal link twists is mapped onto the complete set of joint velocities.

However, the full set of terminal link twists is generally not available and cannot be derived based on velocity relations alone. This was demonstrated for a three-legged PM2E with an internal closed-loop chain. The second insight is that these relations can be complimented with static force relations so that the full set of terminal link twists can be expressed as a function of the known end-effector twists. The static force relations, which appear in the expression as compliance ratios, are required to deal with internal constraints. The possibility for internal constraints is typical for PM2Es and is particularly relevant if the resulting Jacobian is used in a static force analysis, because wrenches applied by the actuators can be transferred to the end-effectors via the internal constraints. The resulting dependency of a Jacobian analysis on mechanical properties is unprecedented in the field of parallel manipulator analysis.

The developed Jacobian analysis was validated using a static force analysis in an example PM2E with three legs and a single internal closed-loop chain. Compliant joints were implemented so that pose-dependent wrenches were applied to the end-effectors without the need of an actuation system. The end-effectors were fixed to an inertial frame via wrench sensors, so that the resulting interaction wrenches could be measured. The interaction wrenches were measured along directions corresponding to the allowed DoFs as well as along constrained directions. These measurements were compared with predicted interaction wrenches based on the developed Jacobian analysis. It was shown that the variability in the measured values is predicted for 99.6% along directions corresponding to the allowed DoFs, and respectively 96.2% and 87.6% for the forces and moments along the constrained directions. Based on these values it is concluded that the example Jacobian analysis is valid.

This paper presented and validated the first example of a Jacobian analysis of a PM2E that takes internal constraints into account. Although the Jacobian analysis presented in this paper was developed for PM2Es with a single internal closed-loop chain and three legs, it was argued that the analysis can be adapted to other PM2Es with relative ease. This is thanks to the structure of the analysis, which can be directly derived from the graph theory representation of a mechanism. As such, the structured approach introduced in this paper sets the stage for the Jacobian analysis of more complex PM2Es.

Acknowledgements

This work was supported by the Dutch Technology Foundation STW (project number 12158), the Natural Sciences and Engineering Research Council of Canada (NSERC)(Grant no. 89715), and the De Breed Kreiken Innovatiefonds, which is managed by the Prins Bernhard Cultuurfonds.

Appendix A. Basis twists, basis wrenches and partial inverse jacobian matrices of the analyzed PM2E

All twists and wrenches introduced in this appendix are expressed in a right-handed Cartesian reference frame connected to the moving body of the serial chain in question, whose origin coincides with the point O. This reference frame is an arbitrary choice, but considered most convenient and logical. Whatever reference frame is chosen, it is important that all vectors are expressed in this same reference frame.

A.1. Full inverse jacobian for first and third leg

The first and third leg are identical RRR serial chains, and are shown in Fig. A.10. Their linearly independent basis twists of permission were obtained as

$$\hat{\$}_{tai,1} = \begin{bmatrix} \hat{\boldsymbol{s}}_i \\ -(l_1\hat{\boldsymbol{r}}_{i,1} + l_2\hat{\boldsymbol{r}}_{i,2} + l_3\hat{\boldsymbol{r}}_{i,3} - \boldsymbol{a}_i) \times \hat{\boldsymbol{s}}_i \end{bmatrix} \tag{A.1}$$

$$\hat{\$}_{tai,2} = \begin{bmatrix} \hat{\boldsymbol{s}}_i \\ -(l_2\hat{\boldsymbol{r}}_{i,2} + l_3\hat{\boldsymbol{r}}_{i,3} - \boldsymbol{a}_i) \times \hat{\boldsymbol{s}}_i \end{bmatrix} \tag{A.2}$$

$$\hat{\$}_{tai,3} = \begin{bmatrix} \hat{\boldsymbol{s}}_i \\ -(l_3\hat{\boldsymbol{r}}_{i,3} - \boldsymbol{a}_i) \times \hat{\boldsymbol{s}}_i \end{bmatrix} \tag{A.3}$$

where $\hat{\$}_{tai,1}$, $\hat{\$}_{tai,2}$, and $\hat{\$}_{tai,3}$ are the basis twists of permission associated to the first, second, and third joints respectively. Furthermore, $\hat{\boldsymbol{s}}_1 = -\hat{\boldsymbol{e}}_2$ and $\hat{\boldsymbol{s}}_3 = \hat{\boldsymbol{e}}_2$, where $\hat{\boldsymbol{e}}_2$ is the unit vector aligned with the Y-axis. The other vectors are illustrated in Fig. A.10, where $\hat{\boldsymbol{r}}_{i,l}$ is the unit vector pointing along the l^{th} link of leg i and $\hat{\boldsymbol{a}}_i$ is the vector pointing from O to the center of the third joint.

Next, taking the conditions posed by [27] into account, a set of basis wrenches of constraint were identified,

$$\hat{\$}_{wci,1} = \begin{bmatrix} \boldsymbol{0}_{3\times1} \\ \hat{\boldsymbol{s}}_i \end{bmatrix} \tag{A.4}$$

$$\hat{\$}_{wci,2} = \begin{bmatrix} \hat{\boldsymbol{e}}_3 \\ \boldsymbol{0}_{3\times1} \end{bmatrix} \tag{A.5}$$

$$\hat{\$}_{wci,3} = \begin{bmatrix} \hat{\boldsymbol{e}}_3 \times \hat{\boldsymbol{s}}_i \\ \boldsymbol{0}_{3\times1} \end{bmatrix} \tag{A.6}$$

Following the methodology described by Huang et al. [23], the set of basis twists of permission described in Eqs. (A.1)–(A.3) and the set of basis wrenches of constraint presented in Eqs. (A.4)–(A.6) can be used to identify a set of basis wrenches of actuation. Namely,

$$\hat{\$}_{wai,1} = \begin{bmatrix} -(l_3\hat{\boldsymbol{r}}_{i,3} - \boldsymbol{a}_i) \times \hat{\boldsymbol{r}}_{i,2} \\ \hat{\boldsymbol{r}}_{i,2} \end{bmatrix} \tag{A.7}$$

$$\hat{\$}_{wai,2} = \begin{bmatrix} -(l_3\hat{\boldsymbol{r}}_{i,3} - \boldsymbol{a}_i) \times \hat{\boldsymbol{f}}_{i,2} \\ \hat{\boldsymbol{f}}_{i,2} \end{bmatrix} \tag{A.8}$$

$$\hat{\$}_{wai,3} = \begin{bmatrix} -(l_2\hat{\boldsymbol{r}}_{i,2} + l_3\hat{\boldsymbol{r}}_{i,3} - \boldsymbol{a}_i) \times \hat{\boldsymbol{r}}_{i,1} \\ \hat{\boldsymbol{r}}_{i,1} \end{bmatrix} \tag{A.9}$$

with

$$\hat{\boldsymbol{f}}_{i,2} = \frac{l_1\hat{\boldsymbol{r}}_{i,1} + l_2\hat{\boldsymbol{r}}_{i,2}}{|l_1\hat{\boldsymbol{r}}_{i,1} + l_2\hat{\boldsymbol{r}}_{i,2}|} \tag{A.10}$$

and finally also a set of twists of constraint was identified,

$$\hat{\$}_{tc_{i,1}} = \begin{bmatrix} \boldsymbol{0}_{3\times1} \\ \hat{\boldsymbol{s}}_i \end{bmatrix} \tag{A.11}$$

$$\hat{\$}_{tc_{i,2}} = \begin{bmatrix} \hat{\boldsymbol{e}}_3 \\ \boldsymbol{0}_{3\times1} \end{bmatrix} \tag{A.12}$$

$$\hat{\$}_{tc_{i,3}} = \begin{bmatrix} \hat{\boldsymbol{e}}_3 \times \hat{\boldsymbol{s}}_i \\ \boldsymbol{0}_{3\times1} \end{bmatrix} \tag{A.13}$$

Eqs. (A.1)–(A.13) were then used to obtain the full inverse Jacobian for the first ($i = 1$) or third leg ($i = 3$),

$$\mathbf{J}_i^{-1} = \begin{bmatrix} \hat{\$}_{wa_{i,1}}^{\top}/(\hat{\$}_{wa_{i,1}}^{\top}\hat{\$}_{ta_{i,1}}) \\ \hat{\$}_{wa_{i,2}}^{\top}/(\hat{\$}_{wa_{i,2}}^{\top}\hat{\$}_{ta_{i,2}}) \\ \hat{\$}_{wa_{i,3}}^{\top}/(\hat{\$}_{wa_{i,3}}^{\top}\hat{\$}_{ta_{i,3}}) \\ \hat{\$}_{wc_{i,1}}^{\top}/(\hat{\$}_{wc_{i,1}}^{\top}\hat{\$}_{tc_{i,1}}) \\ \hat{\$}_{wc_{i,2}}^{\top}/(\hat{\$}_{wc_{i,2}}^{\top}\hat{\$}_{tc_{i,2}}) \\ \hat{\$}_{wc_{i,3}}^{\top}/(\hat{\$}_{wc_{i,3}}^{\top}\hat{\$}_{tc_{i,3}}) \end{bmatrix} \tag{A.14}$$

A.2. Full inverse jacobian for 2nd leg, $\mathbf{J}_2^{-1}$

The second leg is an RRRR serial chains, and a set of linearly independent basis twists of permission was obtained as

$$\hat{\$}_{ta_{2,1}} = \begin{bmatrix} \hat{\boldsymbol{s}}_{2,1} \\ -(l_1\hat{\boldsymbol{r}}_{2,1} + l_2\hat{\boldsymbol{r}}_{2,2} + l_3\hat{\boldsymbol{r}}_{2,3} - \boldsymbol{a}_2) \times \hat{\boldsymbol{e}}_1 \end{bmatrix} \tag{A.15}$$

$$\hat{\$}_{ta_{2,2}} = \begin{bmatrix} \hat{\boldsymbol{s}}_{2,2} \\ -(l_2\hat{\boldsymbol{r}}_{2,2} + l_3\hat{\boldsymbol{r}}_{2,3} - \boldsymbol{a}_2) \times \hat{\boldsymbol{e}}_1 \end{bmatrix} \tag{A.16}$$

$$\hat{\$}_{ta_{2,3}} = \begin{bmatrix} \hat{\boldsymbol{s}}_{2,3} \\ (-l_3\hat{\boldsymbol{r}}_{2,3} - \boldsymbol{a}_2) \times \hat{\boldsymbol{e}}_1 \end{bmatrix} \tag{A.17}$$

$$\hat{\$}_{ta_{2,4}} = \begin{bmatrix} \hat{\boldsymbol{s}}_{2,4} \\ -(l_3\hat{\boldsymbol{r}}_{2,3} - \boldsymbol{a}_2) \times \hat{\boldsymbol{e}}_3 \end{bmatrix} \tag{A.18}$$

where $\hat{\boldsymbol{s}}_{2,1} = \hat{\boldsymbol{s}}_{2,2} = \hat{\boldsymbol{s}}_{2,3} = \hat{\boldsymbol{e}}_1$ is the unit vector aligned with the X-axis, and $\hat{\boldsymbol{s}}_{2,4} = \hat{\boldsymbol{e}}_3$ is the unit vector aligned with the Z-axis.

Subsequently, a set of basis wrenches of constraint was identified as

$$\hat{\$}_{wc_{2,1}} = \begin{bmatrix} \boldsymbol{a}_2 \times \hat{\boldsymbol{e}}_1 \\ \hat{\boldsymbol{e}}_1 \end{bmatrix} \tag{A.19}$$

$$\hat{\$}_{wc_{2,2}} = \begin{bmatrix} \hat{\boldsymbol{e}}_2 \\ \boldsymbol{0}_{3\times1} \end{bmatrix} \tag{A.20}$$

The set of basis twists of permission described in Eqs. (A.15)–(A.18) and the set of basis wrenches of constraint presented in Eqs. (A.19)–(A.20) enabled the identification of a set of basis wrenches of actuation as

$$\hat{\$}_{wa_{2,1}} = \begin{bmatrix} -(l_3\hat{\boldsymbol{r}}_{2,3} - \boldsymbol{a}_2) \times \hat{\boldsymbol{r}}_{2,2} \\ \hat{\boldsymbol{r}}_{2,2} \end{bmatrix} \tag{A.22}$$

$$\hat{\$}_{wa_{2,2}} = \begin{bmatrix} -(l_3\hat{\boldsymbol{r}}_{2,3} - \boldsymbol{a}_2) \times \hat{\boldsymbol{f}}_{2,2} \\ \hat{\boldsymbol{f}}_{2,2} \end{bmatrix} \tag{A.23}$$

$$\hat{\$}_{wa_{2,3}} = \begin{bmatrix} -(l_2\hat{\boldsymbol{r}}_{2,2} + l_3\hat{\boldsymbol{r}}_{2,3} - \boldsymbol{a}_2) \times \hat{\boldsymbol{r}}_{2,1} \\ \hat{\boldsymbol{r}}_{2,1} \end{bmatrix} \tag{A.24}$$

$$\hat{\$}_{wa_{2,4}} = \begin{bmatrix} \boldsymbol{0}_{3\times1} \\ \hat{\boldsymbol{e}}_2 \end{bmatrix} \tag{A.25}$$

where $\hat{f}_{2,2}$ was already described by Eq. (A.10). A set of twists of constraint was then identified as

$$\hat{\$}_{tc_{2,1}} = \begin{bmatrix} \hat{\boldsymbol{e}}_3 \\ \boldsymbol{0}_{3\times 1} \end{bmatrix} \tag{A.26}$$

$$\hat{\$}_{tc_{2,2}} = \begin{bmatrix} \hat{\boldsymbol{s}}_{c,2,2} \\ \boldsymbol{0}_{3\times 1} \end{bmatrix} \tag{A.27}$$

where

$$\hat{\boldsymbol{s}}_{c,2,2} = \frac{1}{\sqrt{(a_{2,y}/a_{2,z})^2 + 1}} [0 \;\; a_{2,y}/a_{2,z} \;\; 1]^\top$$

in which $a_{2,y}$ and $a_{2,z}$ are the elements in the vector $\boldsymbol{a}_2$ aligned with respectively the Y- and Z-axis.

Eqs. (A.15)–(A.27) are then used to obtain the full inverse Jacobian for the second leg,

$$\mathbf{J}_2^{-1} = \begin{bmatrix} \hat{\$}_{wa_{2,1}}^\top / (\hat{\$}_{wa_{2,1}}^\top \hat{\$}_{ta_{2,1}}) \\ \hat{\$}_{wa_{2,2}}^\top / (\hat{\$}_{wa_{2,2}}^\top \hat{\$}_{ta_{2,2}}) \\ \hat{\$}_{wa_{2,3}}^\top / (\hat{\$}_{wa_{2,3}}^\top \hat{\$}_{ta_{2,3}}) \\ \hat{\$}_{wa_{2,4}}^\top / (\hat{\$}_{wa_{2,4}}^\top \hat{\$}_{ta_{2,4}}) \\ \hat{\$}_{wc_{2,1}}^\top / (\hat{\$}_{wc_{2,1}}^\top \hat{\$}_{tc_{2,1}}) \\ \hat{\$}_{wc_{2,2}}^\top / (\hat{\$}_{wc_{2,2}}^\top \hat{\$}_{tc_{2,2}}) \end{bmatrix} \tag{A.28}$$

A.3. Full inverse jacobian for internal serial chains, $\mathbf{J}_{o_1}^{-1}$, $\mathbf{J}_{o_2}^{-1}$, and $\mathbf{J}_{o_3}^{-1}$

In order to develop matrices $\mathbf{J}_{o_1}^{-1}$, $\mathbf{J}_{o_2}^{-1}$, and $\mathbf{J}_{o_3}^{-1}$, first a set of basis twists and basis wrenches is developed for the end-effector serial chains. Both these serial chains are RRR chains and their linearly independent basis twists of permission are

$$\hat{\$}_{ta_{o_{i,1}}} = \begin{bmatrix} \hat{\boldsymbol{s}}_o \\ -(l_o \hat{\boldsymbol{r}}_{o_{i,1}} + l_o \hat{\boldsymbol{r}}_{o_{i,2}} - \boldsymbol{a}_3) \times \hat{\boldsymbol{s}}_o \end{bmatrix} \tag{A.29}$$

$$\hat{\$}_{ta_{o_{i,2}}} = \begin{bmatrix} \hat{\boldsymbol{s}}_o \\ -(l_o \hat{\boldsymbol{r}}_{o_{i,2}} - \boldsymbol{a}_3) \times \hat{\boldsymbol{s}}_o \end{bmatrix} \tag{A.30}$$

$$\hat{\$}_{ta_{o_{i,3}}} = \begin{bmatrix} \hat{\boldsymbol{s}}_o \\ \boldsymbol{a}_3 \times \hat{\boldsymbol{s}}_o \end{bmatrix} \tag{A.31}$$

where $\hat{\$}_{ta_{o_{i,1}}}$, $\hat{\$}_{ta_{o_{i,1}}}$, and $\hat{\$}_{ta_{o_{i,1}}}$ are the basis twists of permission associated to the first, second, and third joints encountered in each end-effector serial chain, going from the first to the second end-effector. The vector $\hat{\boldsymbol{s}}_o$ is the unit vector along the Z-axis, $\hat{\boldsymbol{e}}_3$. This vector, as well as examples of scalars and other vectors in Eqs. (A.29) and (A.31), are illustrated in Fig. A.12, where l_o is the length of all links in the end-effector serial chains. As such, $\hat{\boldsymbol{r}}_{o_{i,l}}$ is the unit vector pointing along the l^{th} link of the i th end-effector serial chain.

Next, taking the conditions posed by Ref. [27] into account, a set of wrenches of constraint was identified. Namely,

$$\hat{\$}_{wc_{o_{i,1}}} = \begin{bmatrix} \boldsymbol{0}_{3\times 1} \\ \hat{\boldsymbol{e}}_3 \end{bmatrix} \tag{A.32}$$

$$\hat{\$}_{wc_{o_{i,2}}} = \begin{bmatrix} \hat{\boldsymbol{e}}_1 \\ \boldsymbol{0}_{3\times 1} \end{bmatrix} \tag{A.33}$$

$$\hat{\$}_{wc_{o_{i,3}}} = \begin{bmatrix} \hat{\boldsymbol{e}}_2 \\ \boldsymbol{0}_{3\times 1} \end{bmatrix}. \tag{A.34}$$

Following the methodology described by Huang et al. [23], the set of basis twists of permission in Eqs. (A.29)–(A.31) and the set of basis wrenches of constraint in Eqs. (A.32)–(A.34) enabled the identification of a set of basis wrenches of actuation as

$$\hat{\$}_{wa_{o_{i,1}}} = \begin{bmatrix} \boldsymbol{a}_3 \times \hat{\boldsymbol{r}}_{o_{i,2}} \\ \hat{\boldsymbol{r}}_{o_{i,2}} \end{bmatrix} \tag{A.35}$$

$$\hat{\$}_{wa_{o_{i,2}}} = \begin{bmatrix} \boldsymbol{a}_3 \times \hat{\boldsymbol{f}}_{o_{i,2}} \\ \hat{\boldsymbol{f}}_{o_{i,2}} \end{bmatrix} \tag{A.36}$$

$$\hat{\$}_{wa_{o_{i,3}}} = \begin{bmatrix} -(l_o \hat{\boldsymbol{r}}_{o_{i,2}} - \boldsymbol{a}_3) \times \hat{\boldsymbol{r}}_{o_{i,1}} \\ \hat{\boldsymbol{r}}_{o_{i,1}} \end{bmatrix} \tag{A.37}$$

with

$$\hat{\boldsymbol{f}}_{o_{i,2}} = \frac{l_o \hat{\boldsymbol{r}}_{o_{i,1}} + l_o \hat{\boldsymbol{r}}_{o_{i,2}}}{|l_o \hat{\boldsymbol{r}}_{o_{i,1}} + l_o \hat{\boldsymbol{r}}_{o_{i,2}}|} \tag{A.38}$$

and finally also a set of twists of constraint was identified,

$$\hat{\$}_{tc_{o_{i,1}}} = \begin{bmatrix} \boldsymbol{0}_{3\times1} \\ \hat{\boldsymbol{e}}_3 \end{bmatrix} \tag{A.39}$$

$$\hat{\$}_{tc_{o_{i,2}}} = \begin{bmatrix} \hat{\boldsymbol{e}}_1 \\ \boldsymbol{0}_{3\times1} \end{bmatrix} \tag{A.40}$$

$$\hat{\$}_{tc_{o_{i,3}}} = \begin{bmatrix} \hat{\boldsymbol{e}}_2 \\ \boldsymbol{0}_{3\times1} \end{bmatrix} \tag{A.41}$$

The basis twists and wrenches presented in Eqs. (A.29)–(A.41) were then used to develop $\mathbf{J}^{-1}_{o_1^2}$, $\mathbf{J}^{-1}_{o_2^3}$, as well as $\mathbf{J}^{-1}_{o_3^1}$. With joint velocity vectors defined as in Eq. (14), and considering that the internal serial chain connecting n_1 and n_2 contains the first two kinematic joints of the first end-effector serial chain, then

$$\mathbf{J}^{-1}_{o_1^2} = \begin{bmatrix} \hat{\$}^{\mathsf{T}}_{wa_{o_{1,1}}} / (\hat{\$}^{\mathsf{T}}_{wa_{o_{1,1}}} \hat{\$}_{ta_{o_{1,1}}}) \\ \hat{\$}^{\mathsf{T}}_{wa_{o_{1,2}}} / (\hat{\$}^{\mathsf{T}}_{wa_{o_{1,2}}} \hat{\$}_{ta_{o_{1,2}}}) \\ \hat{\$}^{\mathsf{T}}_{wa_{o_{1,3}}} / (\hat{\$}^{\mathsf{T}}_{wa_{o_{1,3}}} \hat{\$}_{ta_{o_{1,3}}}) \\ \hat{\$}^{\mathsf{T}}_{wc_{o_{1,1}}} / (\hat{\$}^{\mathsf{T}}_{wc_{o_{1,1}}} \hat{\$}_{tc_{o_{1,1}}}) \\ \hat{\$}^{\mathsf{T}}_{wc_{o_{1,2}}} / (\hat{\$}^{\mathsf{T}}_{wc_{o_{1,2}}} \hat{\$}_{tc_{o_{1,2}}}) \\ \hat{\$}^{\mathsf{T}}_{wc_{o_{1,3}}} / (\hat{\$}^{\mathsf{T}}_{wc_{o_{1,3}}} \hat{\$}_{tc_{1,3}}) \end{bmatrix} \tag{A.42}$$

where the first and second row of Eq. (A.42) map the relative twist between the two end-effectors onto $\dot{q}_{a_{o_1^2,1}}$ and $\dot{q}_{a,o_1^2,2}$, the third row maps that relative twist onto $\dot{q}_{cs,o_1^2,1}$, and rows four to six map it onto $\dot{\boldsymbol{q}}_{c_m,o_2^1}$.

The internal serial chain that connects n_2 and n_3 contains the third kinematic joint of the first end-effector serial chain, so that

$$\mathbf{J}^{-1}_{o_2^3} = \begin{bmatrix} \hat{\$}^{\mathsf{T}}_{wa_{o_{1,3}}} / (\hat{\$}^{\mathsf{T}}_{wa_{o_{1,3}}} \hat{\$}_{ta_{o_{1,3}}}) \\ \hat{\$}^{\mathsf{T}}_{wa_{o_{1,1}}} / (\hat{\$}^{\mathsf{T}}_{wa_{o_{1,1}}} \hat{\$}_{ta_{o_{1,1}}}) \\ \hat{\$}^{\mathsf{T}}_{wa_{o_{1,2}}} / (\hat{\$}^{\mathsf{T}}_{wa_{o_{1,2}}} \hat{\$}_{ta_{o_{1,2}}}) \\ \hat{\$}^{\mathsf{T}}_{wc_{o_{1,1}}} / (\hat{\$}^{\mathsf{T}}_{wc_{o_{1,1}}} \hat{\$}_{tc_{o_{1,1}}}) \\ \hat{\$}^{\mathsf{T}}_{wc_{o_{1,2}}} / (\hat{\$}^{\mathsf{T}}_{wc_{o_{1,2}}} \hat{\$}_{tc_{o_{1,2}}}) \\ \hat{\$}^{\mathsf{T}}_{wc_{o_{1,3}}} / (\hat{\$}^{\mathsf{T}}_{wc_{o_{1,3}}} \hat{\$}_{tc_{1,3}}) \end{bmatrix} \tag{A.43}$$

where the first row maps the relative end-effector twist onto $\dot{q}_{a,o_2^3,1}$, and the second and third rows map the relative end-effector twist onto $\dot{q}_{cs,o_2^3,1}$ and $\dot{q}_{cs,o_2^3,2}$, while again rows four to six map this twist onto $\dot{\boldsymbol{q}}_{c_m,o_2^1}$.

Finally, because in Eq. (54) the internal chain connecting n_1 and n_3 is defined in the opposite direction as the twists in Eqs. (A.29)–(A.31),

$$\mathbf{J}_{o_3}^{-1} = \begin{bmatrix} -\hat{\$}_{wa_{o_{2,1}}}^{\top}/(\hat{\$}_{wa_{o_{2,1}}}^{\top}\hat{\$}_{ta_{o_{2,1}}}) \\ -\hat{\$}_{wa_{o_{2,2}}}^{\top}/(\hat{\$}_{wa_{o_{2,2}}}^{\top}\hat{\$}_{ta_{o_{2,2}}}) \\ -\hat{\$}_{wa_{o_{2,3}}}^{\top}/(\hat{\$}_{wa_{o_{2,3}}}^{\top}\hat{\$}_{ta_{o_{2,3}}}) \\ \hat{\$}_{wc_{o_{2,1}}}^{\top}/(\hat{\$}_{wc_{o_{2,1}}}^{\top}\hat{\$}_{tc_{o_{2,1}}}) \\ \hat{\$}_{wc_{o_{2,2}}}^{\top}/(\hat{\$}_{wc_{o_{2,2}}}^{\top}\hat{\$}_{tc_{o_{2,2}}}) \\ \hat{\$}_{wc_{o_{2,3}}}^{\top}/(\hat{\$}_{wc_{o_{2,3}}}^{\top}\hat{\$}_{tc_{2,3}}) \end{bmatrix} \tag{A.44}$$

Appendix B. Inverse kinematics of 2-DoF PM2E

The inverse kinematics of the example 2-DoF PM2E are developed for each individual serial chain. First the inverse kinematics of the legs are developed, where expression for the angles as shown in Figs. A.10 and 11 can be obtained as

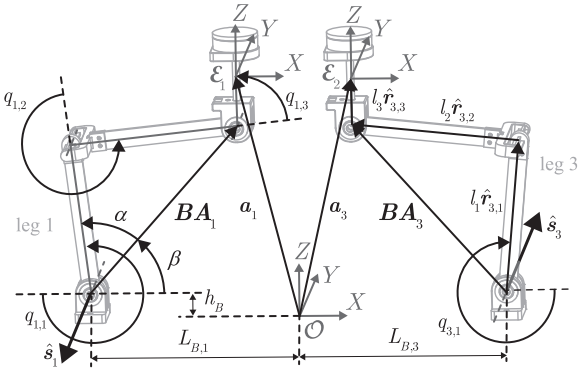

Fig. A.10. Legs one and three and examples of all vectors and scalars that are used in the expression of the basis twists, the basis wrenches, and the inverse kinematics.

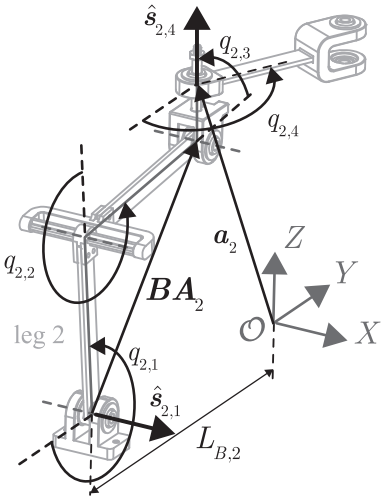

Fig. A.11. Leg two and examples of vectors and scalars that are used in the expression of the basis twists, the basis wrenches, and the inverse kinematics.

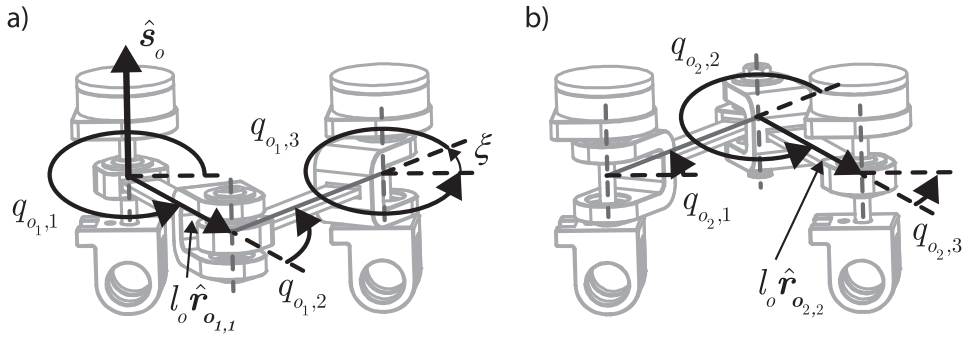

Fig. A.12. a) the first end-effector serial chains and b) the second end-effector serial chain, which is also the third internal serial chain, both with examples of vectors and scalars that are used in the expression of the basis twists, the basis wrenches, and the inverse kinematics.

$$q_{i,1} = \pi + \alpha + \beta q_{i,2} = \begin{cases} \pi + \sin^{-1}\left(\frac{|\mathbf{BA_i}|}{l_2}\sin\alpha\right) & \text{if} \quad |\mathbf{BA_i}|^2 \le l_1^2 + l_2^2 \\ 2\pi - \sin^{-1}\left(\frac{|\mathbf{BA_i}|}{l_2}\sin\alpha\right) & \text{if} \quad |\mathbf{BA_i}|^2 > l_1^2 + l_2^2 \end{cases} \quad q_{i,3} = \frac{7\pi}{2} - q_{i,1} - q_{i,2}$$

where $l_1 = 135$ mm, $l_2 = 150$ mm, and

$$\mathbf{BA_1} = \begin{bmatrix} L_{B,1} + p_{x,e_1} \\ 0 \\ p_{z,e1} - l_3 - h_B \end{bmatrix} \quad \mathbf{BA_3} = \begin{bmatrix} L_{B,3} - p_{x,e_2} \\ 0 \\ p_{z,e2} - l_3 - h_B \end{bmatrix} \quad \mathbf{BA_2} = \begin{bmatrix} L_{B,2} - 0.5\sqrt{(2l_o)^2 - (p_{x,e_2} - p_{x,e_1})^2} \\ 0 \\ p_{z,e1} - l_3 - h_B \end{bmatrix} \alpha = \cos^{-1}\left(\frac{l_1^2 - l_2^2 + |\boldsymbol{BA}|^2}{2l_1|\boldsymbol{BA}|}\right)\beta = \tan^{-1}\left(\frac{BA_z}{BA_x}\right)$$

where $L_{B,1} = L_{B,3} = 187.5$ mm, $L_{B,2} = 242.5$ mm, $l_o = 120$ mm, $h_B = 24$ mm, and where it is assumed that $p_{z,e_1} = p_{z,e_2}$. Next the inverse kinematics of the end-effector serial chains are developed, where expression for the angles as shown in Fig. A.12 can be obtained as

$$q_{o_{1,1}} = 2\pi - \xi, \quad q_{o_{1,2}} = 2\xi, \quad q_{o_{1,3}} = 2\pi - \xi \tag{B.1}$$

$$q_{o_{2,1}} = \xi, \quad q_{o_{2,2}} = 2\pi - 2\xi, \quad q_{o_{2,3}} = \xi \tag{B.2}$$

where

$$\xi = \cos^{-1}\left(\frac{p_{x,e_2} - p_{x,e_1}}{2l_o}\right) \tag{B.3}$$

References

[1] K. Bengtsson, Picking a winner and packing a punch: the second-generation FlexPicker, ABB Rev. 4 (2008) 29–33.
[2] F. Pierrot, V. Nabat, O. Company, S. Krut, P. Poignet, Optimal design of a 4-DOF parallel manipulator: from academia to industry, IEEE Trans. Robot. 25 (2) (2009) 213–224. http://dx.doi.org/10.1109/TRO.2008.2011412.
[3] J. Hesselbach, J. Wrege, A. Raatz, O. Becker, Aspects on design of high precision parallel robots, Assem. Autom. 24 (1) (2004) 49–57. http://dx.doi.org/10.1108/01445150410517183.
[4] L. Bruzzone, G. Bozzini, A flexible joints microassembly robot with metamorphic gripper, Assem. Autom. 30 (3) (2010) 240–247. http://dx.doi.org/10.1108/01445151011061136.
[5] Q.-Z. Ang, B. Horan, H. Abdi, S. Nahavandi, Multipoint haptic guidance for micrograsping systems, IEEE Syst. J. (2014) 1–8. http://dx.doi.org/10.1109/JSYST.2014.2314737.
[6] P. Lambert, J. Herder, A novel parallel haptic device with 7 degrees of freedom, in: 2015 IEEE World Haptics Conference (WHC), Vol. 31, IEEE, 2015, pp. 183–188. http://dx.doi.org/10.1109/WHC.2015.7177711.
[7] F.Y. Chen, Gripping mechanisms for industrial robots, Mech. Mach. Theory 17 (5) (1982) 299–311. http://dx.doi.org/10.1016/0094-114X(82)90011-8.
[8] P.O. Hugo, Industrial Grippers: State-of-the-Art and Main Design Characteristics, in: G. Carbone (Ed.), Grasping in Robotics, 2013, pp. 107–131. http://dx.doi.org/10.1007/978-1-4471–4664-3_5.
[9] M.G. Mohamed, C.M. Gosselin, Design and analysis of kinematically redundant parallel manipulators with configurable platforms, IEEE Trans. Robot. 21 (3) (2005) 277–287. http://dx.doi.org/10.1109/TRO.2004.837234.
[10] B.-J. Yi, Y.N. Heung, H.L. Jae, Y.-S. Hong, S.-R. Oh, I.H. Suh, W.K. Kim, Design of a parallel-type gripper mechanism, Int. J. Robot. Res. 21 (7) (2002) 661–676. http://dx.doi.org/10.1177/027836402322023240.
[11] B.-J. Park, B.-J. Yi, W.-K. Kim, Design and analysis of a new parallel grasper having spherical motion, in: 2004 IEEE/RSJ International Conference on Intelligent Robots and Systems (IROS) (IEEE Cat. No.04CH37566), Vol. 1, IEEE, 2004, pp. 106–111. http://dx.doi.org/10.1109/IROS.2004.1389337.
[12] V. Nabat, M. de la O Rodriguez, O. Company, S. Krut, F. Pierrot, Par4: very high speed parallel robot for pick-and-place, in: IEEE/RSJ International Conference on Intelligent Robots and Systems, IEEE, 2005, pp. 553–558. http://dx.doi.org/10.1109/IROS.2005.1545143.
[13] P. Lambert, H. Langen, R.H.Munnig Schmidt, A Novel 5 DOF Fully Parallel Robot Combining 3T1R Motion and Grasping, in: Volume 2: Proceedings of the

34th Annual Mechanisms and Robotics Conference, Parts A and B, ASME, 2010, pp. 1123–1130. http://dx.doi.org/10.1115/DETC2010-28676.
[14] P. Lambert, J.L. Herder, Parallel robots with configurable platforms: Fundamental aspects of a new class of robotic architectures, Proceedings of the Institution of Mechanical Engineers, Part C: Journal of Mechanical Engineering Science 0 (0) (2015) 1–10. http://dx.doi.org/10.1177/0954406215602511.
[15] S. Tadokoro, Control of parallel mechanisms, Adv. Robot. 8 (6) (1993) 559–571. http://dx.doi.org/10.1163/156855394X00257.
[16] D. Zlatanov, I.A. Bonev, C.M. Gosselin, Constraint singularities of parallel mechanisms, in: IEEE International Conference on Robotics and Automation, Vol. 1, IEEE, 2002, pp. 496–502. http://dx.doi.org/10.1109/ROBOT.2002.1013408.
[17] J.P. Merlet, Jacobian, manipulability, condition number, and accuracy of parallel robots, J. Mech. Des. 128 (1) (2006) 199. http://dx.doi.org/10.1115/1.2121740.
[18] F. Paccot, N. Andreff, P. Martinet, A review on the dynamic control of parallel kinematic machines: theory and experiments, Int. J. Robot. Res. 28 (3) (2009) 395–416. http://dx.doi.org/10.1177/0278364908096236.
[19] A.G.L. Hoevenaars, P. Lambert, J.L.Herder, Generalized Jacobian Analysis of Parallel Manipulators With Multiple End-Effectors, in: Volume 5A: Proceedings of the 38th Mechanisms and Robotics Conference, ASME, 2014, p. V05AT08A081. http://dx.doi.org/10.1115/DETC2014-35675.
[20] H. Sung Kim, H. Lipkin, Stiffness of parallel manipulators with serially connected legs, J. Mech. Robot. 6 (3) (2014) 031001. http://dx.doi.org/10.1115/1.4026333.
[21] A.G.L. Hoevenaars, P. Lambert, J.L. Herder, Jacobian-based stiffness analysis method for parallel manipulators with non-redundant legs, Proceedings of the Institution of Mechanical Engineers, Part C: Journal of Mechanical Engineering Science http://dx.doi.org/10.1177/0954406215602283.
[22] S.A. Joshi, L.-W. Tsai, Jacobian analysis of limited-DOF parallel manipulators, J. Mech. Des. 124 (2) (2002) 254. http://dx.doi.org/10.1115/1.1469549.
[23] T. Huang, H.T. Liu, D.G. Chetwynd, Generalized jacobian analysis of lower mobility manipulators, Mech. Mach. Theory 46 (6) (2011) 831–844. http://dx.doi.org/10.1016/j.mechmachtheory.2011.01.009.
[24] A.G.L. Hoevenaars, P. Lambert, J.L. Herder, Kinematic Design of Two Elementary 3DOF Parallel Manipulators with Configurable Platforms, in: F. Thomas, A. Perez Gracia (Eds.), Proceedings of the 6th International Workshop on Computational Kinematics (CK2013), Vol. 15 of Mechanisms and Machine Science, Springer Netherlands, Dordrecht, 2014, pp. 315–322. http://dx.doi.org/10.1007/978-94-007-7214-4_35.
[25] B.P. Trease, Y.-M. Moon, S. Kota, Design of large-displacement compliant joints, J. Mech. Des. 127 (4) (2005) 788. http://dx.doi.org/10.1115/1.1900149.
[26] A.G.L. Hoevenaars, Wrench measurements on a spatial, passive, 2-DoF Parallel Mech. Two End.-Eff. (2015). http://dx.doi.org/10.4121/uuid:ad6762f8-d652-4ade-a329-a78196a40262.
[27] T. Huang, S. Yang, M. Wang, T. Sun, D.G. Chetwynd, An approach to determining the unknown twist/wrench subspaces of lower mobility serial kinematic chains, J. Mech. Robot. 7 (3) (2014) 031003. http://dx.doi.org/10.1115/1.4028622.